

# The Ekeberg Prize 2021

**Cutting of tantalum: Why it is so difficult and what can be done about it (see page 9)**



Photo: Shutterstock

**Mr Ian Margerison  
joins the T.I.C. team**  
(page 6)



**The Ekeberg Prize  
2021: Winner**  
(page 8)







# T.I.C.'s 62nd General Assembly

(conference and AGM) will take place in

## London, UK

### November 14th - 17th 2021

**Generously sponsored by: Mining Mineral Resources Sarl (Gold) and KEMET Electronics Corp. (Silver)**

Non-members are welcome to attend this event. The T.I.C. General Assembly attracts industry leaders from around the world. Full details are available online at [www.tanb.org](http://www.tanb.org).

Our 2021 conference will explore issues such as:



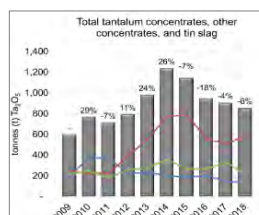
**Capacitors**



**Superalloys**



**Superconductors**



**Statistics**



**And much more**

There will also be two panel discussions about supply chain issues and NORM. Presentations are given in English. All questions about the General Assembly should be sent to Emma Wickens at [info@tanb.org](mailto:info@tanb.org).



The 62nd General Assembly will include the award ceremony for the 2021 Anders Gustaf Ekeberg Tantalum Prize (Ekeberg Prize), the annual international award for excellence in tantalum research and innovation.

The winning publication can be found on page 9 or at <https://www.tanb.org/view/prize>. Information about how to submit a paper for consideration in 2022 is available on the Association's website or from the office.

# President's Welcome

Dear members and friends of the T.I.C.,

I hope this note, as always, finds everyone safe and healthy.

The last few months have been interesting and extremely busy as the T.I.C. staff have been preparing for the upcoming GA62 in London. This same period last year, we were just completing the virtual GA61 and we were starting to look ahead to holding GA62 in person, in Geneva, Switzerland. Unfortunately, as we all know, Geneva had to be pushed out yet another year, in order to accommodate the tour of the Large Hadron Collider at CERN. We expect GA63 and the tour of CERN will be well attended.

Focusing on this year's event in London, UK, entry regulations regarding COVID quarantine and vaccine requirements continue to change, in our favor, as most countries have come off the red list. These changes in requirements, over time, were anticipated when the Executive Committee decided to move GA62 to mid-November rather than try and hold it in the usual October time frame. And while it is unfortunate that many delegates from certain countries will not be able to attend, either because of vaccine requirements or return-home quarantine rules, we are looking forward to a well-attended event. Additionally, there remain a number of member companies that maintain international travel restrictions, also impacting attendance.

As I write, the T.I.C. staff and Meetings Subteam are deeply engaged in finalizing the agenda, working with both presenters and panels, as well as formalizing the set-up of the venue at the Royal Lancaster Hotel in London. The opportunity to hold an in-person event after two years of restrictions is exciting to all involved.

I appreciate the hardships that our members have had to endure over the past few years, and it is unfortunate that all member company delegates will not be in attendance, in London; however, this will not curtail my enthusiasm and anticipation in meeting face-to-face, with member and non-member company delegates, once again.

Please stay well and travel safe.

With sincere regards,

Daniel F. Persico, Ph.D., President

## Contents

The Bulletin No.187

OCTOBER 2021

ISSN 1019-2026



### Features:



The 62nd General Assembly will be held in London, UK

Page 2



The Ekeberg Prize 2021: Winner

Page 8



Mr Ian Margerison joins the T.I.C. team

Page 6



Cutting of tantalum: Why it is so difficult and what can be done about it

Page 9

### Regular articles:

28	Tantalum and niobium patent update	29	Disclaimer
29	Member updates and diary of events	31	Editor's Notes

# 主席致辞



亲爱的T. I. C. 会员和朋友：

我希望这封信能一如既往地让大家感到安全 and 健康。

在过去的几个月里，T. I. C. 的工作人员一直努力为即将在伦敦举行的第62届大会（GA62）做准备，这是有趣而忙碌的。去年同期，我们刚刚完成了第61届虚拟大会（GA61），我们开始期待在瑞士日内瓦举行的第62届大会（GA62）。可惜，我们都知道，为了配合欧洲核子研究中心（CERN）的大型强子对撞机的参观，日内瓦大会不得不再推迟一年。我们预计第63届大会（GA63）和参观欧洲核子研究中心将会有很多人参加。

关注到今年在英国伦敦举行的活动，有关冠状病毒病（COVID）检疫和疫苗要求的入境规定逐步改变，这对我们是有利的，因为许多国家最近已经从红色名单上消失。随着时间的推移，这些要求的变化在执行委员会决定将GA62延迟至11月中旬，而不是试图在惯常的10月时间框架内举行时已经预料到的。遗憾的是，由于疫苗要求或回国后的隔离规定，某些国家的许多代表将无法出席，但是我们仍期待着一个踊跃参加的活动。此外，仍有一些会员公司保持着国际旅行限制，这也对出席率造成一定的影响。

就在我写这篇文章的时候，T. I. C. 的工作人员和会议小组正在深入参与确定议程，与演讲者和小组紧密合作，以及正式确定在伦敦皇家兰开斯特酒店（Royal Lancaster Hotel）的场地设置。在经历了两年的限制后，有机会举办一次实体活动，这对所有参与者来说都是感到兴奋的。

我很欣赏我们的会员在过去几年中面对困难的能力，而遗憾的是，所有会员公司代表都不能出席在伦敦举行的会议；然而，这并不会减少我对再次与会员和非会员公司代表面对面交流的热情和期待。

请保持身体健康，注意旅行安全！

送上真诚的祝福！

丹尼尔·佩尔西科博士（Daniel F. Persico）主席

# Lettre du Président



Chers membres et amis du T.I.C.,

J'espère que cette note, comme toujours, trouvera tout le monde sain et sauf et en bonne santé.

Ces derniers mois ont été intéressants et extrêmement chargés, car le personnel du T.I.C. s'est préparé pour la prochaine GA62 à Londres. L'année dernière, à la même période, nous venions de terminer la GA61 virtuelle et nous commençons à envisager la tenue de la GA62 en personne, à Genève, en Suisse. Malheureusement, comme nous le savons tous, la réunion à Genève a dû être repoussée d'une année supplémentaire, afin de permettre la visite du Grand collisionneur de hadrons au CERN. Nous sommes sûrs que la GA63 et la visite du CERN seront très intéressantes.

En ce qui concerne l'événement de cette année à Londres, au Royaume-Uni, les règles d'entrée concernant la quarantaine COVID et les exigences en matière de vaccins continuent de changer, en notre faveur, car de nombreux pays ont récemment été retirés de la liste rouge. Ces changements d'exigences, au fil du temps, avaient été anticipés lorsque le Comité Exécutif a décidé de déplacer la GA62 à la mi-novembre plutôt que d'essayer de l'organiser à la période habituelle d'octobre. Bien qu'il soit regrettable que les délégués de certains pays ne puissent pas être présents, soit en raison des exigences en matière de vaccins, soit en raison des règles de quarantaine au retour à la maison, nous espérons que l'événement sera bien suivi. En outre, certaines sociétés membres maintiennent des restrictions sur les voyages internationaux, ce qui a également un impact sur la participation.

Au moment où j'écris ces lignes, le personnel du T.I.C. et le Groupe de Travail chargé des réunions sont en train de finaliser l'ordre du jour, de travailler avec les présentateurs et les membres des tables rondes, ainsi que de formaliser la mise en place du lieu de réunion à l'hôtel Royal Lancaster de Londres. L'opportunité d'organiser un événement en personne après deux ans de restrictions est passionnante pour tous les participants.

Je suis conscient des difficultés que nos membres ont dû endurer ces dernières années, et il est regrettable que toutes les sociétés membres ne soient pas représentées à Londres. Toutefois, cela n'entame en rien mon enthousiasme et mon impatience de rencontrer à nouveau les délégués des sociétés membres et non membres.

Je vous prie de prendre soin de vous et de voyager en toute sécurité.

Avec mes sincères salutations,

Daniel F. Persico, Ph.D., Président

# 社長のあいさつ



T. I. C. のメンバーおよび友人の皆様へ。

この便りが、いつものように皆さんの安全と健康を願っています。

ここ数ヶ月、T. I. C. のスタッフはロンドンで開催されるGA62の準備に追われ、非常に忙しく興味深い日々を過ごしています。昨年の同時期、私たちはバーチャルなGA61を終えたばかりで、スイスのジュネーブで直接GA62を開催することを視野に入れ始めていました。しかし残念ながら、CERNの大型ハドロン衝突型加速器（LHC）の見学会を開催するために、ジュネーブでの開催はさらに1年延期されることになりました。GA63とCERNのツアーには多くの参加者が集まることを期待しています。

今年の英国・ロンドンでのイベントに焦点を当てると、COVID検疫とワクチンの必要性に関する入国規制は、最近いくつかの国がレッドリストから外れたことにより、我々に有利な方向に変化し続けています。GA62を通常の10月に開催するのではなく、11月中旬に開催することを実行委員会が決定したのは、このような要件の変化を予測してのことでした。ワクチンの必要性や帰国時の検疫ルールなどの理由で、特定の国から多くの参加者が参加できないのは残念ですが、多くの参加者が集まるイベントになることを期待しています。さらに、海外への渡航を制限している会員企業が多数あり、これも出席率に影響を与えています。

現在、T. I. C. のスタッフとMeetings Subteamは、アジェンダの確定、プレゼンターやパネルとの調整、ロンドンのRoyal Lancaster Hotelでの会場設営などに全力で取り組んでいます。制約の多かった2年後に対面式のイベントを開催できることは、関係者にとって大きな喜びです。ここ数年、会員の皆様にはご苦勞をおかけしており、会員企業の代表者の皆様がロンドンにお越しになれないのは残念ですが、それでも会員企業および非会員企業の代表者の皆様と再び直接お会いできることへの期待と熱意は変わりません。

どうかお元気で、安全な旅をなさってください。

よろしくお願いいたします。

心からのご挨拶を申し上げます。

ダニエル・F・ペルシコ（博士）、社長

# Boas-vindas do Presidente



Caros membros e amigos do T.I.C.,

Espero que esta nota, como sempre, encontre todos em segurança e com saúde.

Os últimos meses têm sido interessantes e extremamente ocupados, uma vez que o pessoal do T.I.C. tem trabalhado na preparação da próxima GA62, em Londres. No ano passado, neste mesmo período, estávamos encerrando a GA61 virtual e vislumbrávamos a realização da GA62 presencial, em Genebra, Suíça. Infelizmente, como todos sabemos, Genebra precisou ser posposta por mais um ano, a fim de permitir a visita ao Grande Colisor de Hádrons no CERN. Esperamos que a GA63 e a visita ao CERN contem com boa participação.

Voltando ao evento deste ano em Londres, Reino Unido: os regulamentos de entrada relativos à quarentena da COVID e aos requisitos de vacinação continuam mudando – a nosso favor –, uma vez que vários países saíram da lista vermelha recentemente. Estas mudanças nos requisitos, ao longo do tempo, foram antecipadas quando o Comitê Executivo decidiu alterar a GA62 para meados de novembro, ao invés de tentar mantê-la no período habitual de outubro. E embora muitos delegados de alguns países não possam estar presentes, infelizmente, seja devido a requisitos de vacinas, seja devido a regras de quarentena no regresso à origem, esperamos por um evento com boa participação. Além disso, ainda existem diversas empresas membro que mantêm restrições de viagens internacionais – o que também afeta o comparecimento.

Enquanto escrevo, o pessoal do T.I.C. e a Subequipe de Reuniões estão profundamente engajados em concluir a agenda, trabalhando tanto com os palestrantes quanto nos painéis, bem como providenciando a organização do local no Hotel Royal Lancaster em Londres. A oportunidade de realizar um evento presencial, após dois anos de restrições, é excitante para todos os envolvidos.

Sou sensível às dificuldades que nossos membros precisaram suportar nos últimos anos, e lamento que nem todos os delegados de empresas membro possam estar presentes em Londres. No entanto, isto não diminuirá meu entusiasmo nem minha expectativa pelo encontro face a face com os delegados de empresas membro e não-membro, mais uma vez.

Por favor, fiquem bem e viajem em segurança.

Com sinceros cumprimentos,

Daniel F. Persico, Ph.D., Presidente



## Mr Ian Margerison joins the T.I.C. team

Earlier this month T.I.C. President Dr Daniel Persico announced the appointment of Mr Ian Margerison as the Association's new Executive Marketing Manager (EMM), succeeding Mr Roland Chavasse who steps down in November.

Mr Margerison has been in the tantalum industry for almost 25 years and brings a wealth of industry knowledge and experience to the role. Ian started his career as a Development Engineer at AVX Tantalum Corporation in Paignton, UK. More recently he spent over a decade at Metalysis, where he led efforts in tantalum additive manufacturing powder development and other key projects.

The EMM is one of the Association's three staff and as such plays an essential role in delivering value to members and representing the Association.

The overarching responsibility of the EMM is to emphasize the T.I.C. brand as the global center of excellence for tantalum and niobium. Activities specific to this goal are leading outreach efforts related to member retention and identifying and signing up new members. Additional responsibilities include design and development of the Association's quarterly and annual publications, the monthly newsletter, as well as maintaining and upgrading the quality of the T.I.C.'s website.

Along with the Technical Officer, the EMM proactively supports the General Assembly and works collaboratively with the Secretary General, Emma Wickens, to ensure T.I.C. members and stakeholders receive the highest possible quality of event and level of service.



Mr Ian Margerison, the Association's new Executive Marketing Manager (EMM)



In 2013 Mr Margerison, then working for Metalysis, was instrumental in arranging for delegates of the 54th General Assembly to visit Metalysis's plant in the UK. Mr Margerison (in a red jacket) is seen here with delegates outside the Metalysis plant (photo: T.I.C.)

As mentioned in the October monthly newsletter, the T.I.C. is also in search mode for a new Technical Officer. In the period this position is vacant, Ian will assume responsibility for publishing the statistics, he will sit on the ITSCI Governance Committee as the T.I.C. representative, and support additional supply chain matters of importance to the T.I.C.

In welcoming Mr Margerison, Dr Persico said "Many of our members know Ian as he has been active in the T.I.C. for many years and sat on the Executive Committee while with Metalysis. The ability to retain an individual of Mr Margerison's caliber and experience is a fortunate event and will allow the Association to forgo the usual "break-in" period. Please extend a hearty congratulations and welcome back to Ian when you see him in London."



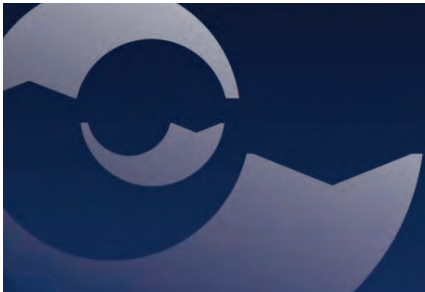
The T.I.C. is part of a consortium studying innovative new ways to recover niobium (Nb), tantalum (Ta) and tungsten (W) from mine by-products and processing waste streams, materials which are currently uneconomical.

If you are interested in learning more about this project visit <https://h2020-tarantula.eu/> or to register your interest contact the T.I.C. at [info@tanb.org](mailto:info@tanb.org).



*The TARANTULA project has received funding from the European Union's EU Framework Programme for Research and Innovation Horizon 2020 under Grant Agreement No 821159.*





# Tantalum and Niobium Suppliers for the Capacitor Electronics, Sputtering Target & Super Alloy Industries Worldwide



tantalum  
73  
**Ta**  
180.95

## Tantalum Products Supplied:

- Tantalum Electron Beam Ingot, Tantalum Vacuum Arc Ingot
- Tantalum Electron Beam Chips, Tantalum Powder
- Tantalum Wire, Tantalum Furnace Parts, Tantalum Strip
- Tantalum Foil, Tantalum Plates – Blanks

niobium  
41  
**Nb**  
92.906

## Niobium products supplied:

- Niobium Electron Beam Ingot, Niobium Vacuum Arc Ingot
- Niobium Electron Beam Chips, Niobium Plate, Niobium Wire
- Niobium Oxide, Niobium Strip, Niobium Foil

## Industries Served:

- Consumer Electronics
- Military Electronics
- Automotive Electronics
- Vacuum Melting
- Sputtering Target
- Deep Drawing
- Medical

**A&R Merchants Inc. is a leader in the supply of conflict free Tantalum & Niobium products**



**A&R Merchants Inc.**  
Tantalum & Niobium

**Visit our website to view our ethics policy**  
**[armerchants.com](http://armerchants.com) • 800-805-9150**



# The Anders Gustaf Ekeberg Tantalum Prize: Winner 2021

*Recognising excellence in tantalum  
research and innovation*



The 2021 Anders Gustaf Ekeberg Tantalum Prize ('Ekeberg Prize') was awarded to a US-Japanese team led by Dr Jason M. Davis of the Center for Materials Processing and Tribology at Purdue University, IN, USA, for its paper "Cutting of tantalum: Why it is so difficult and what can be done about it" published in the journal *International Journal of Machine Tools and Manufacture*. (reprinted on pages 9-26).

## The judges' verdict

Announcing the winner, the independent judging panel led by Dr Axel Hoppe stated that cutting tantalum was a subject which had interested metallurgists for decades and the paper offered important new considerations on the topic.

"In a year when Covid-19 is causing so much disruption and forcing many of us to reconsider what is important in our lives, high on the list of priorities after family and friends must surely be meaningful work, such as moving closer to solving a decades-old challenge?" Dr Hoppe asked.



The winning team (left to right): Dr Jason M. Davis, Dr Mojib Saei, Debapriya Pinaki Mohanty, Dr Anirudh Udupa, Dr Tatsuya Sugihara and Dr Srinivasan Chandrasekar (Photos: by subjects).

The medal for the Ekeberg Prize has been manufactured from pure tantalum metal by the Kazakhstan Mint. The medal is awarded during the T.I.C.'s in-person General Assembly (AGM and conference), which this year will be held in London, UK, from November 14th to 17th. Full details are available at <https://www.tanb.org/event-view/62nd-general-assembly>.

On receiving the Ekeberg Prize, Dr Davis said "We are honoured and humbled that the publication was chosen for the award". The T.I.C. wishes to congratulate all entrants whose papers are challenging the boundaries of current knowledge of tantalum, and which may well lead to significant breakthroughs into exciting new applications of the element.

The authors of the winning paper are Dr Jason M. Davis, Dr Mojib Saei, Debapriya Pinaki Mohanty, Dr Anirudh Udupa, Dr Tatsuya Sugihara, and Dr Srinivasan Chandrasekar. The team mostly work at the Center for Materials Processing and Tribology at Purdue University, IN, USA, while Dr Tatsuya Sugihara is based at the Department of Mechanical Engineering, Osaka University, Japan. Dr Davis also works at the US Special Warfare and Expeditionary Systems Department, Naval Surface Warfare Center in Crane, IN, USA.

Full details about the Ekeberg Prize, including how to submit a paper for the 2022 medal, can be found at [www.TaNb.org](http://www.TaNb.org). **TIC**



# Cutting of tantalum: Why it is so difficult and what can be done about it



Dr Jason M. Davis<sup>ab</sup>, Dr Mojib Saei<sup>a</sup>, Debapriya Pinaki Mohanty<sup>a</sup>, Dr Anirudh Udupa<sup>a</sup>, Dr Tatsuya Sugihara<sup>c</sup>, Dr Srinivasan Chandrasekar<sup>a</sup> at: a) Center for Materials Processing and Tribology, Purdue University, West Lafayette, IN, 47907-2023, USA; b) Special Warfare and Expeditionary Systems Department, Naval Surface Warfare Center, Crane Division, Crane, IN, 47552, USA; c) Department of Mechanical Engineering, Osaka University, Suita, Osaka, 565-0871, Japan. © 2020 by the authors. This article was first published in the *International Journal of Machine Tools and Manufacture*, Volume 157, October 2020, 103607. All views and opinions in this article are those of the authors and not the T.I.C.

## Abstract

Tantalum has long drawn the ire of machinist, being particularly difficult to cut. Often referred to as being 'gummy,' cutting of tantalum is characterized by very thick chips, large cutting forces, and a poor surface finish on the machined surface. These unfavorable attributes of the cutting have usually been attributed to bcc (body centered cubic) tantalum's high strain-hardening capacity, relative softness, and low thermal conductivity; and a small shear plane angle. Here, we show using *in situ* high-speed imaging at low speeds, and *ex situ* chip morphology observations at higher commercial cutting speeds (625 mm/s), that the gummy nature of Ta in cutting, including the large forces and thick chips, is actually due to the prevalence of a highly unsteady plastic flow – sinuous flow – characterized by large-amplitude folding and extensive redundant deformation.

The sinuous flow and the associated folding are much more amplified and extreme in tantalum (chip thickness ratio, 30–50), and with different morphology, than that observed in fcc (face centered cubic) Cu and Al (chip thickness ratio, 10–20), wherein this flow mode was first uncovered. The *in situ* observations are reinforced by force measurements, and chip morphology and cut-surface characterization. The observations also suggest that the sinuous flow, in the same genre of unsteady mesoscale flow modes such as shear banding and segmented flow, is quite prevalent in cutting of highly strain-hardening metal alloys.

By application of a surface-adsorbing (SA) medium, e.g., permanent marker ink, to the initial workpiece surface, we show that sinuous flow can be disrupted and replaced by a more energetically favorable flow mode – segmented flow – with thin chips and >70% reduction in the cutting force. This flow disruption is mediated by a local ductile-to-brittle transition in the deformation zone, due to the action of the SA medium – a mechanochemical (MC) effect in large-strain deformation of metals.

Equally importantly, the MC effect and underlying segmented flow are beneficial also for machined surface quality – producing nearly an order of magnitude improvement in the surface finish, creating a surface with minimal residual plastic strain, and reducing level of material pull-out. Thus, by use of the SA medium and triggering the MC effect, a promising new opportunity is demonstrated for improving the machinability of Ta by ameliorating its gumminess. The results could enhance the viability of Ta for applications such as gun barrel liners – applications for which it has been hitherto considered but discarded due to its poor machining characteristics.

## 1. Introduction

Upon its discovery in 1802, Anders Ekeberg named his new element *tantalum* (now tantalum) after the mischievous Greek demigod Tantalus [1,2]. According to mythology, Tantalus was punished by Zeus for his mischief-making by being forced to stand eternally in a pool of water beneath a fruit tree, with the water always receding before being able to drink and the wind blowing the fruit-bearing branches out of reach [3]. Ekeberg felt the new element had the same tantalizing allure, finding its oxide unreactive with most acids and therefore, making it difficult to separate from tantalite ore [1,2]. For the design engineer and machinist, Ta continues to live up to its name: a metal with some highly desirable properties but notoriously difficult to machine, often attributed to its high strain-hardening capacity. Bcc Ta, like its sister element Nb that lies immediately above it in the periodic table, even though relatively soft (~200 HV) is often described as 'gummy' to cut – i.e., with notoriously poor machinability. Chip formation with Ta is characterized by significant side flow, very thick chips indicative of large strains, large forces, and poor surface finish due to seizing, tearing, and unclear chip separation [4–8]. These characteristics have been attributed to a small shear plane angle and occurrence of unsteady flow [6,7].

While Ta is extraordinarily difficult to machine, there are many important applications for which it is well-suited over other metals, due to its high corrosion resistance (similar to that of glass) and refractory nature (melting point ~3000 °C) [9].

Some of its uses, and potential uses, include jet engine and missile components, penetrator projectiles, nuclear reactor components, chemical processing equipment, and biomedical implants (hip and knee replacement parts, skull plates, dental implants) [9,10]. The poor machinability of Ta has, however, precluded its wider use. For example, an application for which Ta has been considered but not implemented, due to its poor machinability, is in explosively-bonded, gun-tube liners in small arms. Over a decade ago, the United States Army Research Laboratory (ARL) partnered with industry and national laboratories to research and develop such a liner to improve gun barrel life. In 2008, an industry partner began work on implementing crown broach cutters to rifle prototype Ta-lined gun barrel tubes. A crown broach set was used that consisted of 60 individual cutter heads, each containing 9 pairs of teeth. Each pass of the broach was used to cut 18 grooves and increase the depth of the grooves by 10  $\mu\text{m}$ . Two barrel sections were broached; but each time, a tooth on the broach broke. Failure analysis revealed galling and metal build-up on the teeth as the cause of tool breakage. The galling was attributed to any number of different issues: dull or chipped tooth, insufficient cooling at the tooth, chip interference during the cutting process, and/or misalignment of the broach. Conventional rifling of the barrels was subsequently abandoned in search of other machining processes [11]. Unfortunately, little research has been done to understand and address the poor machinability of Ta, in the past two decades, beyond the earlier parametric studies of cutting conditions (e.g., speeds, feeds, tool rake angle, and cutting fluid) on tool life [12,13].

The difficulty of machining Ta has been ascribed to various factors. First, Ta although soft and quite ductile, work-hardens extensively, albeit, at a slow rate [4,14]. This results in extensive deformation in chip formation and, often, also in a built-up edge near the tool tip [8,12]. Second, the low thermal conductivity and diffusivity of Ta, causes the heat from the shear zone to disperse slowly [4]. To prevent excess heat generation, low cutting speeds are recommended, typically in the range of 0.5–1.5 m/s for finishing cuts in turning [12,13]. Lastly, friction at the tool-chip interface is often blamed for the thick chip, arising as it were from a small shear angle [7,8]. Friction also amplifies the built-up edge and heat generation. While these factors serve as signatures of the poor machinability, their underlying causes require a basic understanding of the mechanics of large strain deformation in Ta.

Tantalum is certainly not the only metal described as being gummy to cut – various commercially pure (CP) metals such as Cu, Al and Nb in the annealed or partially worked state; and stainless steels and Ni alloys, also share that moniker, consistent with their large strain-hardening. In machining, these materials too form thick chips, and exhibit large cutting forces and poor surface finish for a range of cutting parameters – typically low to moderate speed and undeformed chip thickness. It has been shown, recently, using high-speed *in situ* imaging of the cutting, that the gummy behaviour of CP Cu and Al, both fcc metals, is due to chip-formation occurring by a large-amplitude folding process, that is fundamentally different from chip-formation by conventional simple-shear with a well-demarcated shear zone/plane [15,16]. In the light of this finding, it is prudent to ask if a similar (folding) type of chip formation mechanism is responsible for the extraordinarily poor machinability and gummy nature of Ta.

In this study, we examine the plastic flow dynamics behind why Ta is so difficult to cut, and how its machinability could be improved by control of these flow dynamics. The flow dynamics are examined using high-speed *in situ* imaging of the cutting, complemented by force and surface quality measurements, and chip morphology observations. We capture details of the chip-formation deformation at high resolution and decipher the reason(s) as to why Ta is gummy to cut. We go further and show that, by exploiting a recently uncovered mechanochemical (MC) effect with common media such as inks and glues [17,18], the cutting of Ta is greatly improved, with >70% reduction in cutting force, and an order of magnitude improvement in surface finish. Equally importantly, the mechanochemically machined surface is much less deformed – a state that may be called “minimally strained”. The results offer a means for solving not only the Ta machining problem, but also that is prevalent with other similar bcc metals like Nb. In the process, a highly unsteady flow mode – sinuous flow with large-amplitude folding – uncovered earlier in cutting of pure Cu and Al (fcc metals) is also shown to be prevalent in cutting of Ta, a model bcc system. The structure of this paper is as follows. The experimental details are provided in Sect. 2. This is followed by observations and analysis of flow modes (Sects. 3.1–3.5). Discussion and implications of the results are presented in Sect. 4, followed by concluding remarks (Sect. 5).

## 2. Experimental

To examine plastic flow modes in machining of Ta, experiments were carried out with a linear, plane-strain (2D) cutting system (Fig. 1a). In this system, the metal workpiece in the form of a rectangular plate is moved at constant velocity  $V_0$  relative to a tool of rake angle  $\alpha$ ; the tool cutting edge is normal to  $V_0$  and the set depth  $h_0$  is the undeformed chip thickness. The cutting results in a chip of nominal thickness  $h_c$ , which moves up the rake face with velocity  $V_c$ . The cutting was observed *in situ* and recorded using a high-speed CMOS camera (pco.dimax) coupled to an optical microscope (Nikon Optiphot), see Fig. 1b. The chip-formation zone – the region of interest – was illuminated by a 120-W halogen lamp.



A glass block was clamped against the workpiece along its cutting length. This constraint ensured that there was no side-flow of the workpiece material during cutting, thus ensuring plane-strain; and that the tool and workpiece were in the same focal plane for the imaging. The imaging configuration provided a spatial resolution of  $1.4\ \mu\text{m}$  per pixel and a recording area as large as  $1296 \times 1296$  pixels; the images were recorded at 500 fps. The high-speed image sequences were post-processed using a Digital Image Correlation (DIC) technique, enabling quantitative analysis of the deformation in terms of displacements, velocities, flow lines, and strain rate and strain fields [16,19]. The three components of the resultant force, viz., cutting, thrust, and lateral, were measured using a three-axis piezoelectric dynamometer (Kistler 9254, natural frequency  $\sim 2\ \text{kHz}$ ). Quality of the cut surface was characterized in terms of topography using a large-area 3D optical profilometer (Zygo NewView 8300), and mechanical state by residual plastic strain and indentation hardness.

The Ta was procured in an initially annealed state, with hardness of 200 HV. The elemental composition of the Ta, as determined by energy-dispersive X-ray spectroscopy (EDX) at multiple voltages (10, 15, 20 kV), was confirmed to be 94% Ta, falling under the category of commercially pure (CP) Ta. The material was annealed by heating in vacuum to  $1100\ ^\circ\text{C}$  and holding for 90 min; the sample was furnace-cooled, under vacuum, to room temperature in 24 h. An optical micrograph of the annealed microstructure is shown in Fig. 2. The metallographic procedure for the sample consisted of first being mounted on top of a cold mount acrylic resin (Lecoset 100) cast using super glue. Polishing was performed using sandpaper with progressively finer grit (600-, 1200-, and then 2000-grit), followed by  $3\text{-}\mu\text{m}$  and  $1\text{-}\mu\text{m}$  diamond paste. The sample was then polished using a GIGA900 Vibratory Polisher for 6 h using colloidal silica solution. Etching was carried out with a mixture of sulfuric acid: nitric acid: hydrofluoric acid = 30:10:10 by volume. The sample was swabbed with cotton soaked in the acid mixture. After swabbing the sample 10 times, residual acid on the sample was washed quickly with tap water, and the sample surface was dried with compressed air. The process was repeated three times for a total of 30 swabbings. The microstructure is clean, with no precipitates or second phase particles visible even at higher magnifications. The grain size, as determined by the lineal intercept method, was  $40\ \mu\text{m}$  in the shorter direction, and with aspect ratio of 2.8.

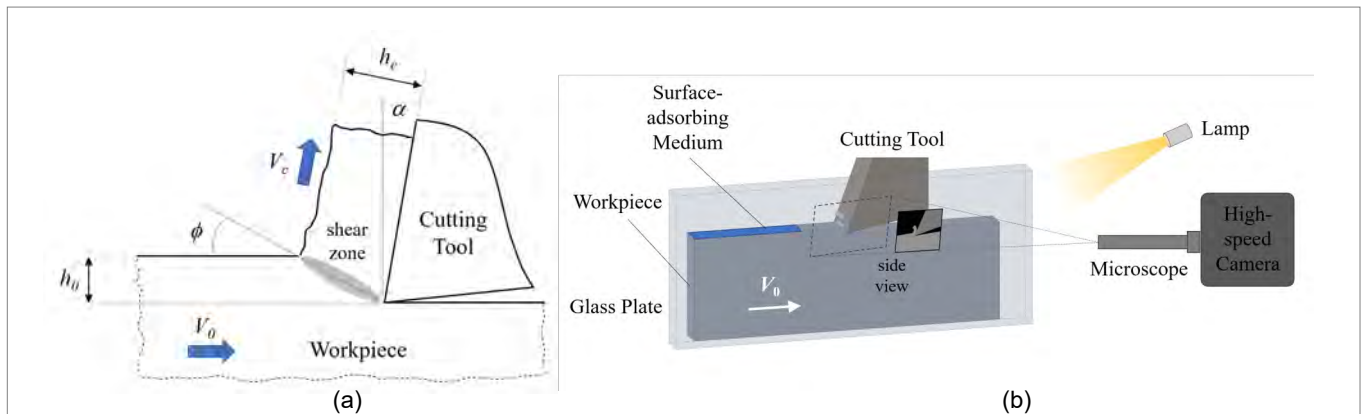


Figure 1. Plane-strain cutting configuration used in experiments. (a) Schematic showing key parameters and classical shear zone model of deformation. (b) *In situ* imaging of material flow in the deformation zone using a high-speed camera coupled to an optical microscope. The side surface of the metal workpiece being imaged is constrained by a glass block to prevent transverse material flow and ensure a common focal plane.

Samples for the linear cutting experiments were prepared in plate form, approximately  $80\ \text{mm}$  length  $\times$   $25\ \text{mm}$  height  $\times$   $6\ \text{mm}$  width, by milling. The surface on which the cutting was done was left untouched during the sample preparation as to ensure that it was still in the annealed condition. Cutting was done along the  $80\text{-mm}$  length, using a HSS tool with  $\alpha = 10^\circ$ ,  $V_0 = 2\ \text{mm/s}$  and nominal  $h_0$  of  $40\text{--}50\ \mu\text{m}$ . The exact value of  $h_0$  was measured in every experiment. A few experiments were performed at  $h_0$  of  $30$  and  $90\ \mu\text{m}$  to determine effect of undeformed chip thickness on flow dynamics. The cutting edge was wider than the workpiece width of  $6\ \text{mm}$ , ensuring plane-strain. A secondary set of experiments was done at higher  $V_0$  of  $625\ \text{mm/s}$ , in a rotary plunge-turning configuration, with a  $25.4\text{-mm}$  diameter bar of annealed Ta. This speed is typical of commercial machining of Ta. For this set,  $\alpha$  was  $0^\circ$ ,  $h_0 \sim 50\ \mu\text{m}$  (feed/rev), and the tool/chip width was  $3.8\ \text{mm}$  ( $>10h_0$ ), again ensuring plane-strain. The edge radius of the tool in all cases was  $<5\ \mu\text{m}$ . All the cutting experiments were done dry without use of any fluid.

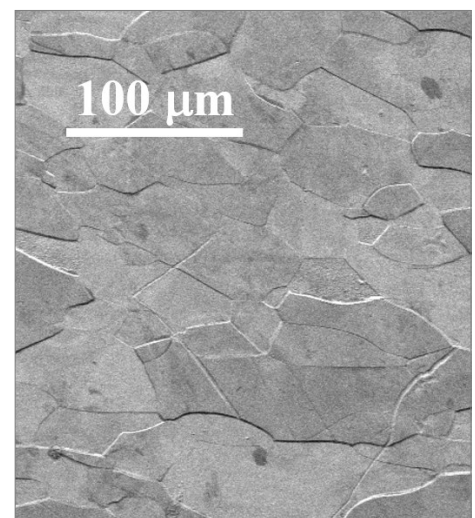


Figure 2. Ta workpiece microstructure

### 3. Results

The high-speed *in situ* imaging of the chip formation, together with the force, chip and surface quality characterization, have provided comprehensive characterization of plastic flow dynamics; and the role of the flow field in influencing energy dissipation and workpiece surface deformation.

#### 3.1. Chip morphology

An overview of the chip-formation flow in Ta is readily obtained from SEM observations of chip morphology. Fig. 3a shows a side cross-sectional view of the chip for  $V_0 = 2$  mm/s. The chip is very thick, with a chip thickness ratio ( $\lambda = h_c/h_0$ ) of 38 at the maximum; this represents an extraordinary level of thickening and plastic straining. The free (back) surface of the chip consists of a series of ridges that span the width of the chip, see Fig. 3b. Each ridge has a mushroom-like appearance in the side view (Fig. 3a). The widths of the individual ridges, which resemble folds, are 70  $\mu\text{m}$ , see inset to Fig. 3b.

The chip produced at the higher  $V_0$  of 625 mm/s (Fig. 4) also has a very similar morphology, with the chip free surface consisting of mushroom-like ridges of width  $\sim 100$   $\mu\text{m}$ . Fig. 4a is a side cross-sectional view of one of the very thick ridged regions ( $\lambda$  of 51), analogous to Fig. 3a; these regions were found to occur at regular intervals along the chip length. The ridged regions were interspersed with very local regions of chip fracture, likely occurring by failure of the thick ridged segments when the forces reach a critical (large) value. Multiple overlapping/interweaving ridges are seen to span the width and length of the chip (Fig. 4b). By comparing the chip morphologies of Figs. 3 and 4, it is clear that the chip formation mechanics is essentially unaltered in the speed range of 2 mm/s to 625 mm/s; the latter speed is quite typical of commercial cutting speeds for Ta [12]. In fact, this type of ridged or folded chip morphology has been reported elsewhere also - in turning of Ta at a cutting speed of 1000 mm/s for rake angles of  $-5^\circ$ – $25^\circ$  [6,7]; and in machining of Nb at similar speeds [20].

#### 3.2. Flow characterization: Sinuous flow and folding

In order to understand the origin of the thick chip (equivalently, the gumminess) and the texture on the chip free-surface, we observed the dynamics of chip formation and underlying material flow, *in situ*, using a high-speed camera. Fig. 5a–f shows six frames selected from a high-speed image sequence of the cutting, with background color map highlighting the effective (von Mises) strain field. The development of the flow/deformation can be understood by following the motion of a series of surface points demarcated in the images, and the streaklines superimposed onto the images. (Note: A streakline is a line formed by the loci of all particles that have passed continuously through a fixed point; at some instant in time, the particles are marked and connected with a line [21].). At time  $t_0$  (frame 1 – Fig. 5a), a bump begins to develop on the workpiece surface ahead of the advancing tool, between the surface points  $P_1$  and  $P_2$ . These points appear to serve as pinning points (extremities) between which the bump develops. Upon advance of the tool (frame 2 – Fig. 5b,  $\Delta t = 0.2$  s), two additional bumps, denoted as  $P_2 - P_3$  and  $P_3 - P_4$ , are nucleated behind the original bump ( $P_1 - P_2$ ). The first bump ( $P_1 - P_2$ ) meanwhile has grown in amplitude, with its axis (dotted line) rotating counterclockwise, and sheared into a fold. Similarly, after another 0.2 s (frame 3 – Fig. 5c) and as the tool advances further, bump  $P_3 - P_4$  develops into a fold, by similar rotation and shearing, with significant growth in amplitude. This process of bump formation, and subsequent development of the bump, into a fold is a recurring event (quasi-periodic) as seen in frames 3–6 (Fig. 5c–f), where several other folds are highlighted along with their nucleating bumps and pinning points ( $P_4$  through  $P_8$ ). The bumps and folds vary in amplitude, much more so than in Cu and Al; for example,  $P_5 - P_6$  shows a bump/fold that is much greater in amplitude than the others. A total of seven distinct folds have formed over a 1-s duration (Fig. 5). Collectively, the folds, once fully developed, create a fan-like structure with the axes of the folds converging to a common location near the tip of the tool, see for example Fig. 5c and e. The strain within the chip is greatest at this point of convergence, with values in the range of 8–10 (background color map, Fig. 5). Along the chip free surface, each fold is seen as a mushroom-like structure in the side view (Figs. 3a and 4a) and as ridge like feature in the plan view of the chip free surface (Figs. 3b and 4b).

Other *in situ* observations carried out over a longer duration of cutting, showed the deformed chip to typically progressively increase in thickness by piling-up of the folds (fan-like structure, Fig. 5f), thus resulting in a folded segment such as shown in Figs. 3a and 4a. When such a folded segment became very thick, it fractured, locally, due to the forces reaching very large values, both at the low and high speeds. This deformation/fracture process was observed to repeat, resulting in the chip consisting of a series of folded segments, with the fold-axes of each segment fanning out from the tool edge, separated (or interspersed) by very local regions of fracture. The repeated folding is the reason for the large and varying chip thickness, as well as the ridge-shaped morphology of the chip free-surface. This chip morphology is also quite different from that arising from folding in Cu and Al; in the latter instances, while the chip was quite thick (chip thickness ratio of 10–20), it was made up of a continuous stack of folds (rather than folded segments) and the variations in chip thickness were much less so than in Ta.



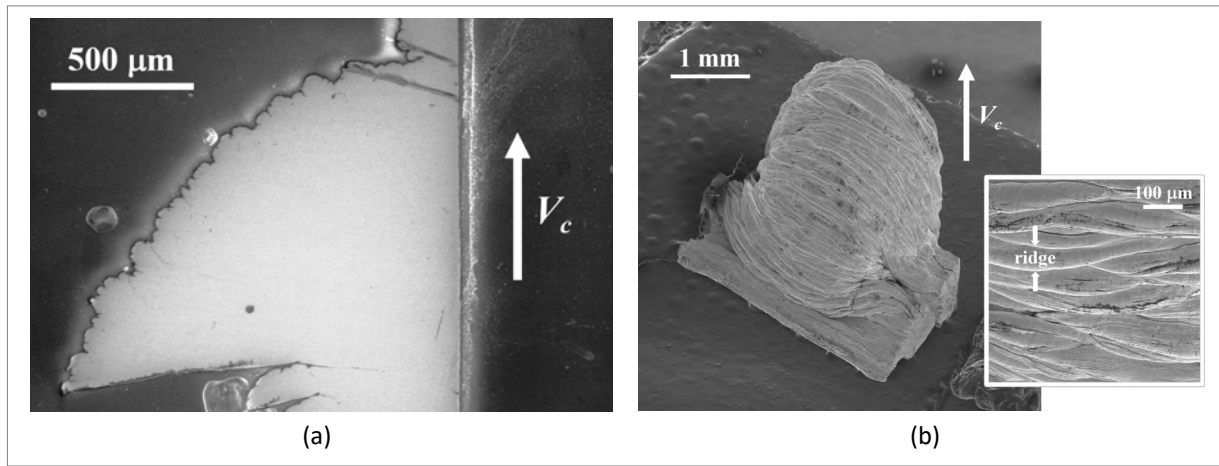


Fig. 3. Morphology of Ta chip by scanning electron microscopy (SEM). (a) Side cross-sectional (length  $\times$  thickness) view of a (folded) chip segment showing extraordinary level of thickening (chip thickness ratio of 38), and mushroom-like features on chip free-surface. (b) Free (back) surface of the chip showing stack of ridges and severe thickening. Inset is close-up view of the ridges on the chip free-surface. The ridges run mostly straight across the chip width but with some interlacing.  $V_0 = 2 \text{ mm/s}$ ,  $\alpha = 10^\circ$ ,  $h_0 = 40 \text{ }\mu\text{m}$ .

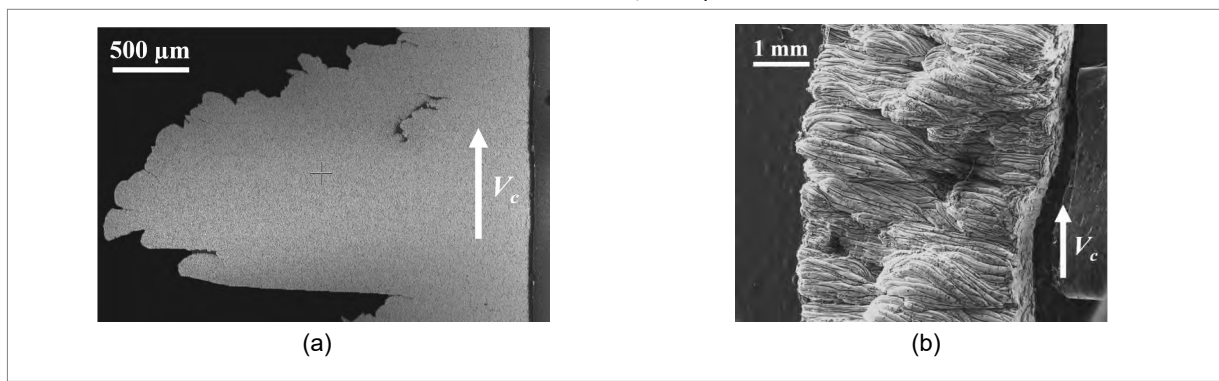


Fig. 4. Morphology of chip obtained from turning of Ta by SEM. (a) Side cross-sectional (length  $\times$  thickness) view of folded chip segment showing similar thickening (chip thickness ratio of 51), and mushroom-like features on free surface, as in low-speed cutting. (b) Free (back) surface of chip showing multiple stacks of ridges.  $\alpha = 0^\circ$ ,  $h_0 = 50 \text{ }\mu\text{m}$ ,  $V_0 = 625 \text{ mm/s}$ .

The plastic flow process resulting in the folded chip has significant vortex-like components, as revealed by the wavy (sinewy) nature of the streaklines shown in Fig. 5. This is a direct consequence of the repeated bump and fold formation, and the folds which stack up together to form the chip. Furthermore, the strain field arising from this flow is highly heterogeneous, with the chip strains ranging from 4 to 10 (color in Fig. 5); the highest strains of 8–10 occur in the vicinity of the tool edge. This type of highly unsteady, vortex-like flow has been termed as sinuous flow [15,16]. If the chip formation is viewed as a material shape-change via a plastic deformation process, then it is clear this sinuous flow with folding is characterized by extensive redundant deformation. While similar sinuous flow has been observed earlier in cutting of annealed commercially pure fcc metals like Cu and Al [15,17, 22], the Ta chip formation represents perhaps the most extreme case of folding observed to date, and, the first case, in a bcc system. And it is the folding that gives rise to the “ridge-like” structures observed on the chip free-surface in Figs. 3 and 4. Thus the ridges are just folds that are caused by the vortex-like sinuous flow. The observations of sinuous flow in Ta attest to the generality of occurrence of this type of flow, especially with metals that show significant strain-hardening capacity. Indeed, sinuous flow has also been observed recently in machining of stainless steels and niobium. The sinuous flow chip-formation highlighted in Fig. 5 is fundamentally different from the textbook (conventional) picture of chip formation, usually depicted as arising from smooth laminar flow due to a shear plane/zone. Rather, it is an unsteady flow mode in the same genre as shear banding [23–25] and segmented flow [26–28].

An important consequence of the folding-induced redundant deformation is the high specific force and energy dissipation in the primary deformation zone (Note: Specific force is force divided by the product of chip width and undeformed chip thickness.). In fact, the measured specific force for machining of Ta in our cutting experiments reaches a maximum of 15,800 MPa (see Sec. 3.4). For reference, the specific force in finish turning of hard steels ( $\sim 60 \text{ HRC}$ ,  $700 \text{ HV}$ ) is  $\sim 8150 \text{ MPa}$ , for a  $10^\circ$  rake angle and  $40 \text{ }\mu\text{m}$  undeformed chip thickness [29,30]; note that the annealed Ta is only  $\sim 30\%$  as hard as these steels. Such large forces also cause tool-life in Ta cutting to be low [8]. The gummy nature of Ta, typified by the thick folded chips and large forces, is thus a consequence of chip formation by sinuous flow.

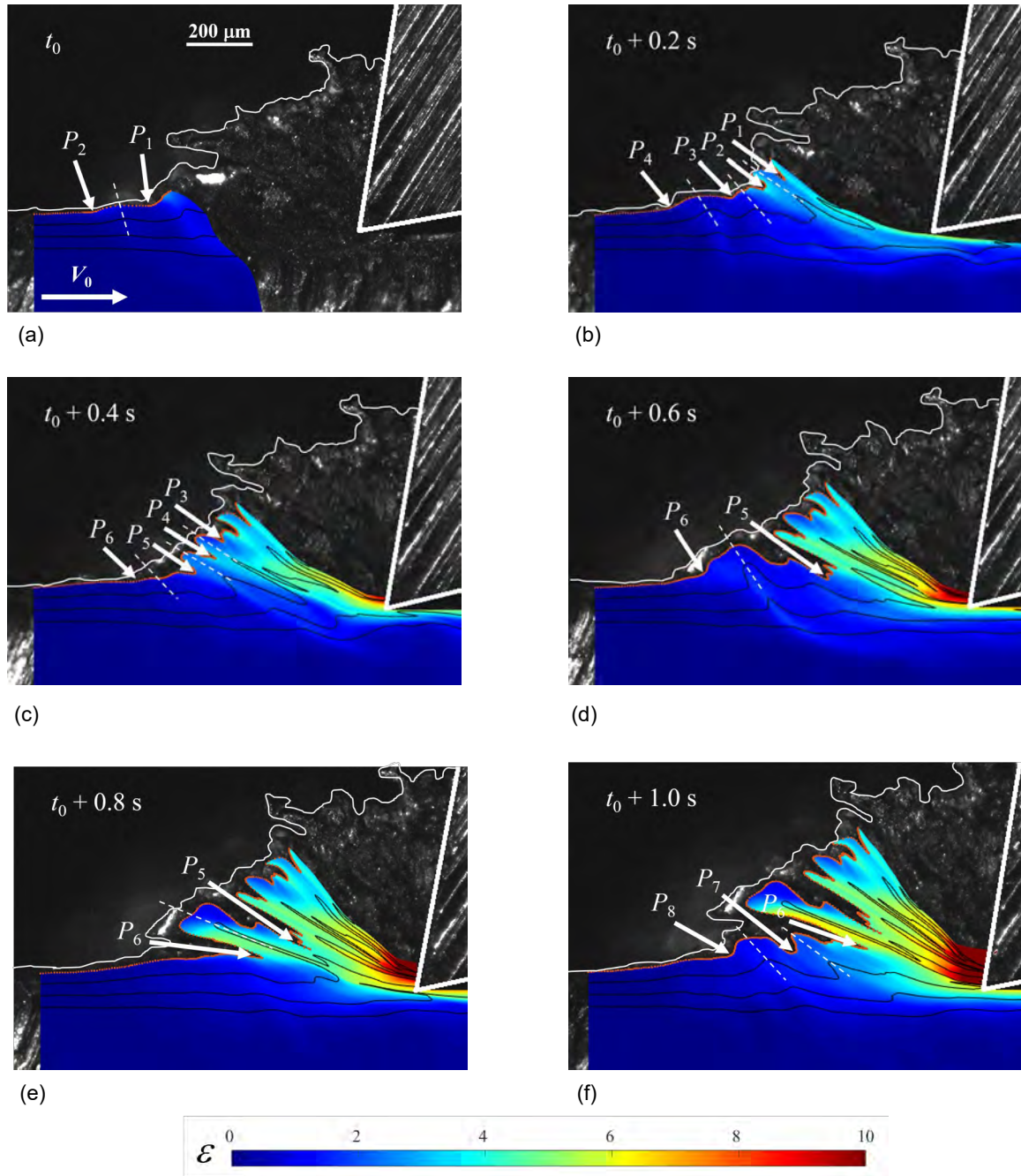


Fig. 5. High-speed *in situ* image sequence of development and progression of sinuous flow with folding in Ta. Overlaid onto the image are the strain field (background color), which is quite heterogeneous; and a few, highly-sinewy streaklines which show significant vortex-like (rotation) components of flow. (a) At some time  $t_0$ , a small bump develops on the workpiece surface ahead of the tool between pinning points  $P_1$  and  $P_2$ . This bump formation involves differential grain deformation, and resembles plastic-buckling of a thin surface layer. (b) After 0.2 s, the pinning points  $P_1$  and  $P_2$  move closer together, with the axis of the bump rotating counter-clockwise. During this period, multiple additional bumps nucleate on the surface between  $P_2 - P_3$  and  $P_3 - P_4$ . (c) At 0.4 s, bumps  $P_1 - P_2$ ,  $P_2 - P_3$ , and  $P_3 - P_4$  have all increased in amplitude, and rotated/sheared to become folds. Another fold  $P_4 - P_5$  has developed as well, along with a new bump forming between  $P_5 - P_6$ . (d) As the tool advances, bump  $P_5 - P_6$  continues to grow in size. (e) At 0.8 s, bump  $P_5 - P_6$  has progressed into a fold by the usual rotation/shearing. (f) After 1.0 s, bumps  $P_6 - P_7$  and  $P_7 - P_8$  have formed, for a total of seven distinct buckling events. The folds create a fan-like structure that spreads out from the tool tip. The strain field is highly heterogeneous with strains ranging from 10 (tool-tip) to 4 elsewhere in the chip body.  $\alpha = 10^\circ$ ,  $h_0 = 40 \mu\text{m}$ ,  $V_0 = 2 \text{ mm/s}$ . (For interpretation of the references to color in this figure legend, the reader is referred to the Web version of this article.)

It should be noted that while the details of the sinuous flow such as folding and vortex-like displacements have been established using observations at high ( $1 \mu\text{m}$ ) resolution, albeit at low speeds, the prevalence of this flow mode at higher speeds typical of commercial machining practice has been inferred mainly from *ex situ* chip morphology observations. By comparing Figs. 3 and 4, it is clear that the chip morphology has the same folded appearance, with mushroom-like structures at the chip free surface, under both low and high speed cutting conditions.



Similar folded-chip morphologies, as well as cutting instabilities (e.g., chip thickness oscillation), typical of sinuous flow, have been reported also at even higher speeds ( $\sim 1$  m/s) than used here, in both Ta and Nb [6–8,20]. However, direct *in situ* mapping of unsteady flows at speeds  $>0.5$  m/s, and at high spatial resolution similar to that achieved here ( $\sim 1$   $\mu\text{m}$ ), requires solution of multiple experimental challenges – e.g., imaged area size vis-à-vis resolution, illumination issues, ensuring plane strain in deformation zone via application of side constraint – that go well beyond just use of high camera framing rates. Efforts are ongoing to address these challenges, including via possible use of marker techniques which have been successful even at speeds of 5 m/s [24]. High spatial-resolution mapping of deformation is essential for capturing mesoscale details of unsteady flow development (e.g., shear bands, segmentation, sinuous), unlike for the case of laminar flow [24,31,32].

It is instructive to compare and contrast the attributes of the folding and sinuous flow in bcc Ta with those observed in annealed or partially worked (fcc) Al and Cu. The folding and mushroom-like features on the chip free surface seen in the Ta cutting (Fig. 5) are broadly similar to those observed in Al and Cu, and characteristic of the sinuous flow mode. For Al and Cu, each fold originates as a bump, bound by pinning points, on the workpiece free surface ahead of the cutting tool. This bump then develops then into a fold by a rotation and shearing process very much analogous to that in Ta shown in Fig. 5 [15,16]. Note that in this type of unsteady flow, there is no shear plane that can be demarcated. Hence thick chip formation cannot be a consequence of a small shear plane angle as has been suggested [7,8]. Furthermore, the sinuous flow in Ta is much more extreme than in the Al and Cu, as seen from the chip thickness ratio. This ratio reaches values of 40–50 in Ta, whereas it is typically 10–20 for the Cu and Al. However, in the Ta, the deformed chip progressively increases in thickness during cutting due to a piling-up of folds in the form of a fan-like structure (Fig. 5f); this results in a chip segment comprised of numerous folds, i.e., a folded chip segment. When such a folded segment becomes very thick (Figs. 3a and 4a), it fractures due to the forces reaching very large values; this deformation/fracture process then repeats resulting in the chip consisting of a series of thick folded segments separated by very local regions of fracture.

### 3.3. Enhancing cutting by suppressing sinuous flow and folding

The flow characterization has demonstrated that sinuous flow with folding is the principal reason for the poor machinability and gumminess of Ta. Consequently, attempts to facilitate or improve the machining of Ta must focus on disrupting the sinuous flow mode and replacing it with a more favorable mode that involves less energy dissipation in chip formation. Prior work suggests that this could potentially be accomplished to some degree by varying the initial state of the workpiece material or via changes in the deformation geometry. It has been found with other gummy metals like Cu and Al that pre-straining the workpiece material (to reduce its strain-hardening capacity) prior to the cutting, by a deformation process like rolling, can reduce the extent of the sinuous flow, and, sometimes, even fully replace it with a more favorable smooth laminar flow [33,34]. The forces with laminar flow are much smaller, and the surface finish is simultaneously much improved. Another strategy is to make the tool rake angle quite positive – a change in the deformation geometry – which also promotes laminar flow with its attendant benefits [8]. In fact, this has been recommended also for Ta machining, where relatively thin chips have been reported at large rake angles [6,7]. But positive rake angle tools often result in lower tool life, a problem also with Ta [8], because of geometrical weakening of the tool edge. Hence, these approaches to mitigate the effects of sinuous flow are not always viable options or even preferred. An alternate, more general method, to suppress sinuous flow and improve the cutting is therefore desirable.

A possible general method to suppress sinuous flow in Ta is suggested by recent work that has uncovered a new mechanochemical (MC) phenomenon (effect) in cutting of soft and/or highly strain-hardening metals [17,18]. The occurrence of (mechano) chemical effects in plasticity and fracture has for long been known, see for example discussions of effects associated with the names of Roscoe, Joffe, Rehbinder and Bangham [35–40]. These effects pertain largely to changes in mechanical response of solids when their surface is exposed to action of chemical media. The recently uncovered MC effect is characterized by a ductile-to-brittle transition occurring in the cutting zone of metals undergoing sinuous flow – this transition being affected by chemical media that are adsorbed onto the metal surface. One dramatic manifestation of this phenomenon occurs when surface-adsorbing (SA) media, often household items such as inks, dyes and glues, are applied to the initial workpiece surface of gummy metals like Al and Cu prior to the cutting. The normally active sinuous flow mode is replaced by segmented flow that is dominated by fracture. This change in flow mode occurs via a local ductile-to-brittle transition in the deformation zone – the development of the sinuous flow being arrested by onset of quasi-periodic fracture. Importantly, the segmented flow results in much smaller cutting forces, lower chip strains, and improved quality of the cut surface [17,18]; hence, it is a much more favorable mode for chip formation, including chip management [41]. It is worth noting that this flow transition is not lubrication-induced, for the SA medium is not present anywhere near the tool-chip interface but only on the initial surface of the workpiece ahead of the chip formation zone and advancing tool (Fig. 1b).

Three general categories of SA media have been identified based on the efficacy of the MC effect, and compatibility with the metal surface [17]. The first type (Type-I) is media whose action is fairly material-agnostic, meaning they show the aforementioned MC effect with a variety of different gummy metals. Such media display strong physical adsorption to the metals. This type tends to be common, relatively benign media used in general adhesion applications or for marking metals. Examples of such media (used in prior experiments with Cu and Al) by trade name include Scotch restickable glue stick (a N-Vinylpyrrolidinone-based adhesive), Scotch super glue gel (a cyanoacrylate-based adhesive), Gorilla super glue (a polyurethane-based adhesive), Sharpie permanent marker, Dykem metal marking ink, and Paper Mate Liquid Paper correction fluid. Note that the inks in this category are essentially dyes, and not colloidal inks. The second type (Type-II) of SA media that exhibit the MC effect are those whose action is material-specific, meaning they have a chemical affinity for only a certain metal – likely undergoing a chemical reaction with the metal surface – and change the flow of media. An example of this type is isopropyl alcohol and its effect on aluminum [18]. The last type of media (Type-III) does not demonstrate the MC effect at all, for this type adsorbs poorly or not at all to the metal surface. Examples in this category include distilled water, variously commonly used metal-cutting lubricants (e.g., Mobil 1), and paraffin wax.

### 3.3.1. Cutting with an ink-film (SA medium)

Since Ta during cutting displays sinuous flow and extreme folding, even more so than Cu and Al, we hypothesized that it would respond to SA media much the same as these gummy metals do – that is a mechanochemical effect would be manifest. To test this hypothesis, we decided to carry out cutting experiments with ultrathin films (~200 nm thick) of Sharpie permanent marker ink as the SA medium. This ink had been identified as an effective Type-I medium in previous studies and, furthermore, it is easily applied to the workpiece surface. More information concerning the physical and chemical properties of this ink, its capacity to develop a film, and characterization of ink-film thickness is provided in Appendix A.

The experiments with the ink were conducted in the linear cutting configuration (Fig. 1b), with the nominal cutting conditions being  $\alpha = 10^\circ$ ,  $V_0 = 2$  mm/s and  $h_0 = 40$   $\mu\text{m}$ , unless otherwise specified. This configuration permits for the probing of both the sinuous flow and its response to an SA medium, concurrently, in the same experiment (cutting pass), by applying the SA medium to only one half of the workpiece surface along its cutting length (Fig. 1b). In the present case, the ink film, ~200 nm thick (see Appendix A), was applied to the latter half of the cutting length. Thus in a single pass, the tool is cutting the uncoated surface of the workpiece first followed by the ink-coated surface.

### 3.3.2. Flow dynamics and chip morphology

Fig. 6 is a SEM image showing a cross-sectional (length  $\times$  thickness) side view of the chip from one of the experiments ( $h_0 = 50$   $\mu\text{m}$ ) in which the ink was applied to one half of the length. The cutting of the initial (uncoated) half of the workpiece produces the familiar folded, fan-like chip arising from sinuous flow, akin to that described earlier (Fig. 5). The thickness of the chip is ~1.7 mm at the base, which represents a nearly 34-fold (very large) thickening of the material during the deformation process. The folding causes the chip to have large variations in its thickness, as well as in the free surface of the chip having an irregular mushroom-like morphology when viewed from the side (Fig. 6). These mushroom structures correspond to the ridges noted earlier. Similar mushroom-like structures are also apparent in the chip produced at 625 mm/s (Fig. 4a).

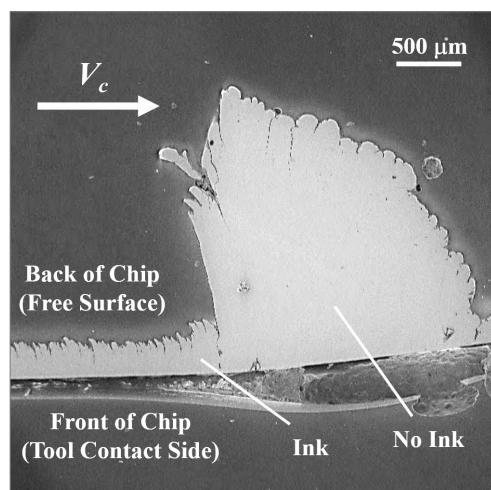


Fig. 6. SEM image of chip (length  $\times$  thickness, cross-section) produced by cutting Ta workpiece that is coated with an ink medium only along part of its cutting length. The initial part of the cutting length is uncoated. The non-inked region shows a very thick chip (~34-fold thickening), with mushroom-like free-surface morphology, formed by sinuous flow and folding. In contrast, the chip from the inked-region is quite thin (~5-fold thickening) and forms by segmentation flow. A sharp change in the chip morphology and underlying flow from sinuous-folding from  $\alpha = 10^\circ$ ,  $h_0 = 50$   $\mu\text{m}$ ,  $V_0 = 2$  mm/s



In direct contrast, the morphology and structure of the chip from the latter part of the cut, the ink-coated region, is fundamentally different (Fig. 6). Firstly, the chip now is much thinner ( $\sim 250 \mu\text{m}$ ) corresponding to  $\lambda \sim 5$ . Secondly, the chip shows a segmented morphology, with cracks running across a significant fraction of the chip thickness; this morphology is very reminiscent of the well-known, saw-tooth chip. Furthermore, the segments are fairly regularly spaced (quasi-periodic), running continuously (straight) across the width of the chip. This may be seen from Fig. 7a and b which are SEM images of the chip free surface. Closer examination of the saw-teeth reveals that each of them is made up of smaller segments (Fig. 7b). Fig. 7c is an optical microscope image of the chip surface in contact with the tool rake surface. Cracks are apparent on this surface all along the chip width, with the crack spacing ( $\sim 270 \mu\text{m}$ ) coinciding with the spacing of the segments. This shows that the segments are a consequence of a fracture process, wherein the cracks appear to have initiated on the chip free-surface (see ensuing *in situ* observations) and propagated towards the tool edge and at least partially through the chip thickness. The cross-sectional view of the chip in Fig. 6 does not clearly show this aspect of the crack feature, most likely due to the discontinuous nature of the cracks; That is, it is difficult to discern the actual beginning and end of the large saw-tooth segments from the cross-sectional view.

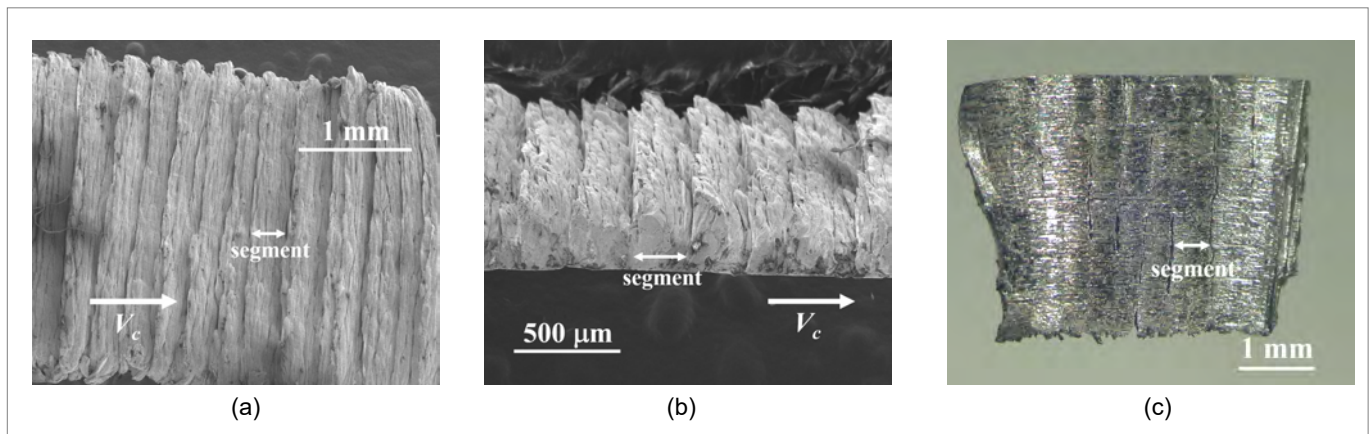


Fig. 7. SEM images of morphology of segmented chip in cutting of Ta with ink applied to the workpiece surface. (a) Free (back) surface of the chip showing segments, that are somewhat regularly spaced, running straight across the chip width without any meandering. (b) Higher magnification, perspective view of the chip free-surface (same as in (a)) showing straight segments, and saw-tooth chip. (c) Chip surface in contact with the tool rake surface showing cracks.  $\alpha = 10^\circ$ ,  $h_0 = 40 \mu\text{m}$ ,  $V_0 = 2 \text{ mm/s}$ .

High-speed imaging was successful in unravelling the mechanics of segmented chip formation and in showing the segmentation (fracture) to in fact originate on the chip free-surface (Fig. 8). The frames in the figure show crack initiation and growth over a 0.41 s cutting duration, with the motion of points  $P_1$  and  $P_2$  describing the segmentation. At time  $t_0$  (Fig. 8a),  $P_1$  and  $P_2$  are very close in proximity and on opposite sides of the nucleating crack. After 0.17 s (Fig. 8b), the crack has grown in length (distance between  $P_1$  and  $P_2$  has increased) with  $P_2$  becoming the crack tip. After an additional 0.24 s (Fig. 8c), the crack substantially elongates and widens. This fracture process repeats periodically leading to the segmented chip. The *in situ* and ex situ observations, taken together, show that the ink film not only disrupts the sinuous flow development but causes the chip to form by a quasi-periodic fracture process that is perhaps more efficient from an energy standpoint, and for chip management [41], compared to the sinuous-flow case.

Fig. 9a and b are SEM images that show effect of  $h_0$  on chip formation and segmentation. For  $h_0$  of  $50 \mu\text{m}$  and  $90 \mu\text{m}$ , the corresponding deformed chip thickness ( $h_c$ ) values are  $\sim 230 \mu\text{m}$  and  $380 \mu\text{m}$ , respectively. Sometimes, the actual segmentation lengths are somewhat difficult to discern from these cross-sections due to the preponderance of smaller segments within larger ones. However, for  $h_0$  of  $50 \mu\text{m}$  and  $90 \mu\text{m}$ , features of similar appearance and size are separated by a distance of  $60 \mu\text{m}$  and  $100 \mu\text{m}$ , respectively. Thus, an 80% increase in  $h_0$  translates into a roughly 65% increase in  $h_c$  and segment spacing, suggesting a self-similar scaling of the segmentation. Fig. 9a and b also reveal that at the larger  $h_0$ , the cracks that initiate on the free surface of the chip do not propagate all the way to the chip under-surface, as with  $h_0 = 40 \mu\text{m}$ , but are arrested part way into the chip thickness. This aspect of the segmentation is also very similar to what has been observed in segmented chip formation in conventional (no ink application) cutting of materials such as copper, brass and Mg [28]. The much thinner segmented chip, which is indicative of reduced deformation levels, and the key role of fracture in effecting the segmentation (Figs. 7 and 8), together suggest that the deformation energy and forces should be much smaller when cutting with the ink-medium applied.

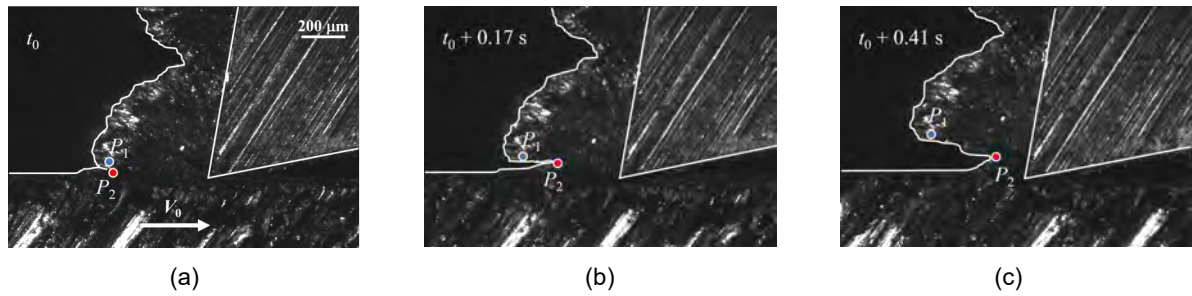


Fig. 8. Frames from a high-speed image sequence showing development of segmentation flow in Ta cutting with the ink-medium applied. (a) A crack initiates on the chip free surface ahead of the advancing tool at time  $t_0$ .  $P_1$  and  $P_2$  are close together on opposite sides of the incipient crack. (b) The crack grows after 0.17 s with the distance between  $P_1$  and  $P_2$  increasing, and  $P_2$  becoming the crack tip. (c) With further advance of the tool (0.41 s), the crack rapidly opens up and propagates towards the tool tip. This crack nucleation repeats periodically creating a segmented chip.  $\alpha = 10^\circ$ ,  $h_0 = 30 \mu\text{m}$ ,  $V_0 = 2 \text{ mm/s}$ .

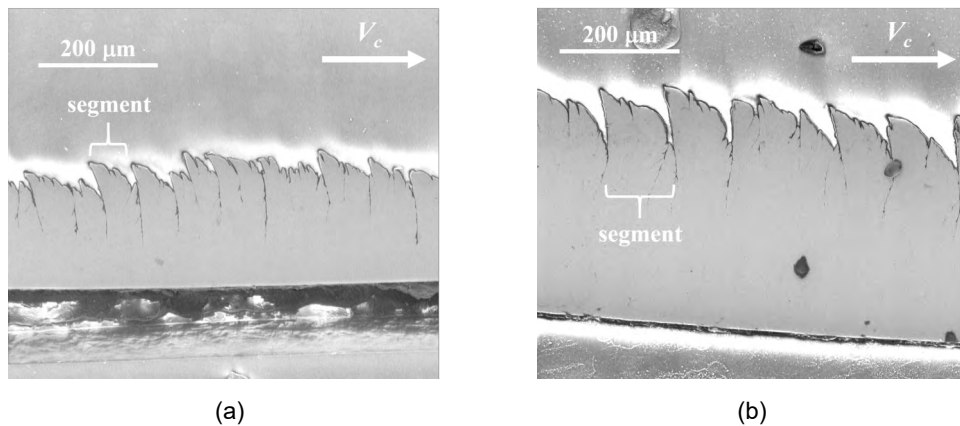


Fig. 9. Scaling of the segmentation with  $h_0$  when cutting Ta in presence of SA (ink) medium. (a) An undeformed chip thickness  $h_0$  of  $50 \mu\text{m}$  results in a deformed (segmented) chip with mean thickness  $230 \mu\text{m}$ . The mean spacing between the segments is  $\sim 60 \mu\text{m}$ . (b) An undeformed chip thickness  $h_0$  of  $90 \mu\text{m}$  results in deformed (segmented) chip with thickness  $380 \mu\text{m}$ , and segment spacing  $\sim 100 \mu\text{m}$ . Note that both the thickening of the chip and the segment spacing scale linearly with  $h_0$ .  $\alpha = 10^\circ$ ,  $V_0 = 2 \text{ mm/s}$ .

### 3.4. Forces

One of the distinguishing quantitative attributes of the mechanochemical effect, observed in prior work with Cu and Al, is a large decrease in the cutting and thrust forces [16–18]. As an aside, this aspect has also been confirmed by others [42] using the same ink media as us [16]. A dramatic reduction in forces was also observed in the cutting of Ta (ink). Fig. 10 is a plot of forces showing this major reduction in specific cutting ( $F_c$ , power) and thrust ( $F_t$ ) force components. In the uncoated region, the first part of the cut,  $F_c$  climbs steadily to a maximum value of approximately  $15,800 \text{ N/mm}^2$ ; for reference, the corresponding  $F_c$  for finish turning of a hardened steel (hardness  $\sim 60 \text{ HRC} > 3 \times \text{Ta hardness}$ ) is nearly 50% smaller,  $\sim 8150 \text{ N/mm}^2$ , for the same rake angle and undeformed chip thickness [29,30]. These large forces are an important contributor to high tool wear in Ta cutting [8]. Upon encountering the coated region, the latter part of the cut,  $F_c$  abruptly and steeply drops to an approximate average value of  $3740 \text{ N/mm}^2$ , a reduction of  $\sim 75\%$ . This major reduction in  $F_c$  is undoubtedly due to the local ductile-to-brittle transition in flow, from sinuous to segmented, that is induced by the SA medium (Sharpie ink). Furthermore, the  $F_c$  in the coated region oscillates with time, with oscillation (half) amplitude that is 15% of the average. Using a periodogram, the dominant frequency in the  $F_c$  oscillation was determined to be  $0.59 \text{ Hz}$ . This matches well with the segmentation frequency of the chip ( $\sim 0.6 \text{ Hz}$ ) determined by metallography. The origin of the oscillation is as follows: as an individual segment is forming,  $F_c$  increases continuously until a fracture event occurs, leading to a sudden decrease in the force. This process of periodic segmentation with corresponding force drops was found to occur throughout the region in which the SA medium was applied. The force oscillations (Fig. 10) and chip morphology (Fig. 7b) observations also reinforce what we have reported earlier – that when segmentation occurs in cutting, with the segments running straight across the chip width, then this segmentation is also manifested as a force drop. The same is not always true if the segments meander across the chip width [28].



The thrust force component  $F_t$  also decreases, and oscillates similarly as  $F_c$ , due to the Sharpie medium application. However, the  $F_t$  reduction is less pronounced, only ~65%. Since  $F_t$  has more to do with the contact conditions at the tool-chip interface, this observed reduction in  $F_t$  implies that the segmentation-type flow, a consequence of the MC effect, is also more favorable from a friction standpoint. However, in order to recognize this, it is important to examine the  $F_t$  magnitude and not the ratio  $F_t/F_c$  which is often taken as a measure of the cutting friction (coefficient). In the present case, this ratio for the sinuous flow (~0.35) is actually much smaller than for the segmentation case (~0.56), and would lead to an erroneous interpretation of how the tool-chip friction is influenced by the flow.

Another demonstration of the  $F_c$  reduction due to the MC effect can be found in Fig. 11. In this case, the forces were measured when cutting a Ta workpiece that had been only periodically marked with the Sharpie ink. The ink itself was applied as bands of width ~5 mm, alternating with non-inked regions also of 5 mm width (inset shows the bands on the chip free surface after deformation). Here, the  $F_c$  fluctuates between high (uncoated) and low (coated) values, with the force fluctuations matching the spatial frequency of the ink bands, confirming the characteristic force-reduction attribute of the MC effect.

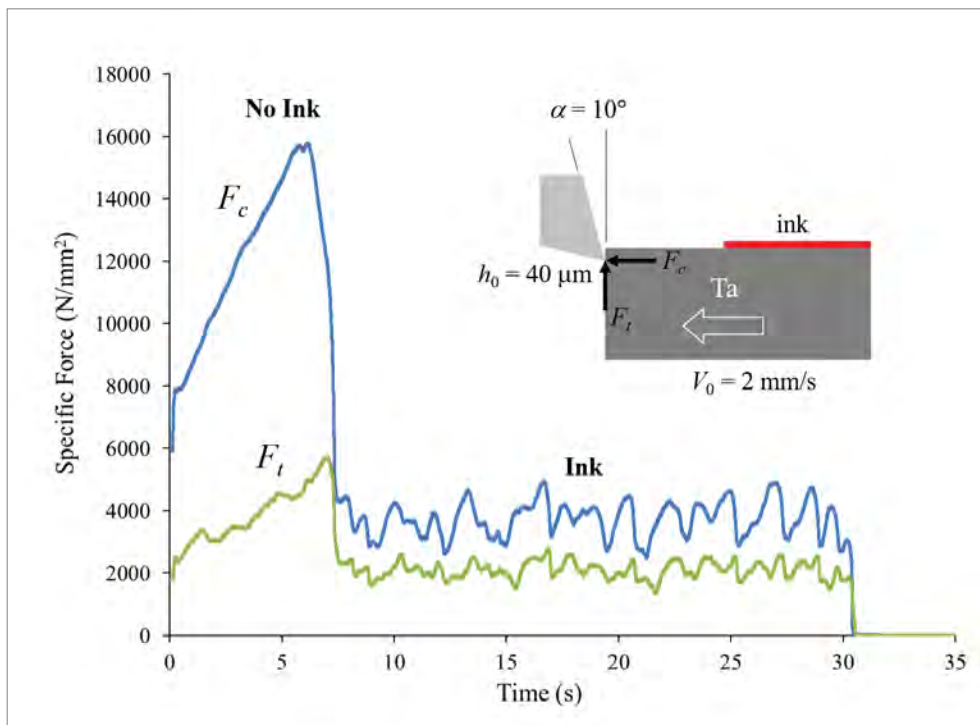


Fig. 10. Specific cutting ( $F_c$ ) and thrust ( $F_t$ ) forces when cutting Ta workpiece coated with ink only along part of its cutting length (see inset).  $F_c$  in the uncoated region is very high due to the sinuous flow. A dramatic (~75%) decrease in this force is seen when cutting over the inked region with segmented flow. Also, in the uncoated region,  $F_c$  is rapidly increasing. In contrast, in the inked region,  $F_c$  is not only small but steady, with small periodic fluctuations that are a consequence of the segmentation; it is reflective of a more stable cutting process.  $\alpha = 10^\circ$ ,  $h_0 = 40 \mu\text{m}$ ,  $V_0 = 2 \text{ mm/s}$ .

### 3.5. Surface quality

The quality of the machined surface was characterized in terms of surface topography (roughness, tears and material pull-out), hardness and residual plastic (deformation) strain, to determine whether there were any major benefits from the MC effect.

#### 3.5.1. Surface topography

Accompanying the force reduction, due to the MC effect, is a pronounced, nearly order of magnitude, improvement in the surface topography of the newly (cut) created workpiece surface. Fig. 12 shows 3D surface profiles along the Ta workpiece length, obtained via optical profilometry, for the inked and non-inked regions; this profile was put together by stitching together a number of individual profiles. As is apparent, the surface corresponding to the non-inked region has a markedly rough texture – valleys with ridges. This suggests significant material pull-out during the cutting. Importantly, the arithmetical mean height roughness  $S_a$  of the surface corresponding to the inked region is ~2  $\mu\text{m}$ , an approximately 9-fold improvement over that of the non-inked surface ( $S_a \sim 18 \mu\text{m}$ ).

It should be noted that this  $S_a$  value also includes contributions from material pull-out. The tool marks seen along the length of the surface in the inked region indicate active cutting, not plowing. Furthermore, this part of the cut surface is largely devoid of defects like tears and material pull-outs in contrast to the non-inked region. The topography improvement is also evident in the line profiles provided in Fig. 12.

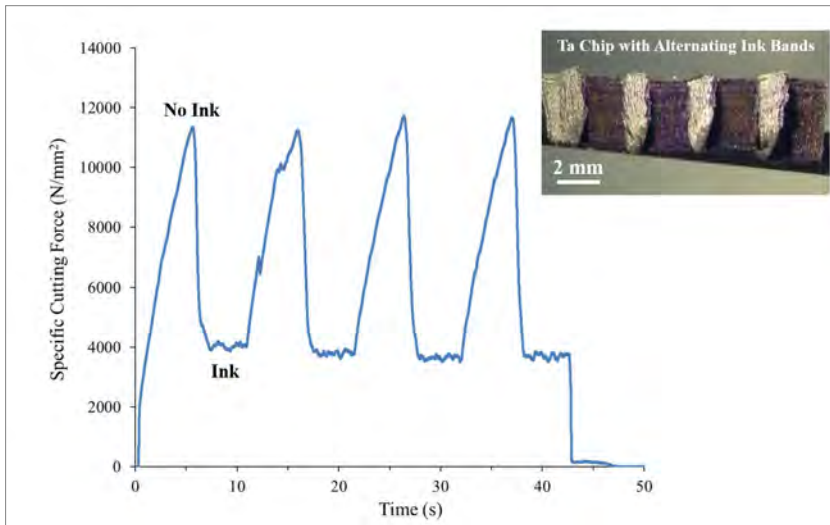


Fig. 11. Specific cutting force trace when cutting Ta sample inked at regular intervals along the cutting length. See inset chip picture for how ink (dark) and non-ink regions alternate. The force is high in the non-inked region (sinuous), but quite small in the inked region (segmented) bands.  $\alpha = 20^\circ$ ,  $h_0 = 40 \mu\text{m}$ ,  $V_0 = 2 \text{ mm/s}$ .

### 3.5.2. Surface strain

The DIC analysis of high-speed image sequences was also used to map the residual plastic strain field on the workpiece surface in the wake of the tool [16], i.e., the cut surface. This was done by integrating the strain rate field along path lines that traverse the deformation zone and become part of the workpiece [16]. These strain values were then averaged to determine the strain at a given depth. Fig. 13 shows the variation of residual plastic strain with depth from the cut surface for the sinuous (no ink) and segmented (ink) flow cases. The surface produced under conditions of sinuous flow is intensely deformed, with a large surface strain,  $\epsilon \sim 5.5$ . In contrast, the workpiece surface produced under conditions of segmented flow enabled by the MC effect shows a much smaller surface strain,  $\epsilon \sim 1.7$ . Additionally, the depth of the deformed layer on the cut surface is also much reduced for the segmented flow case. If we use  $\epsilon = 0.5$  as the cut-off value to describe the extent of the deformed layer, then the depth of the strained layer is  $\sim 30 \mu\text{m}$  for the segmented flow and  $\sim 90 \mu\text{m}$  for the sinuous flow. Thus the MC effect is valuable also for producing a cut surface with much less residual plastic strain, in fact a “minimally strained” surface. This should be beneficial for enhancing fatigue life of the surface, especially since fatigue crack nucleation is strongly influenced by the plastic strain state [43,44].

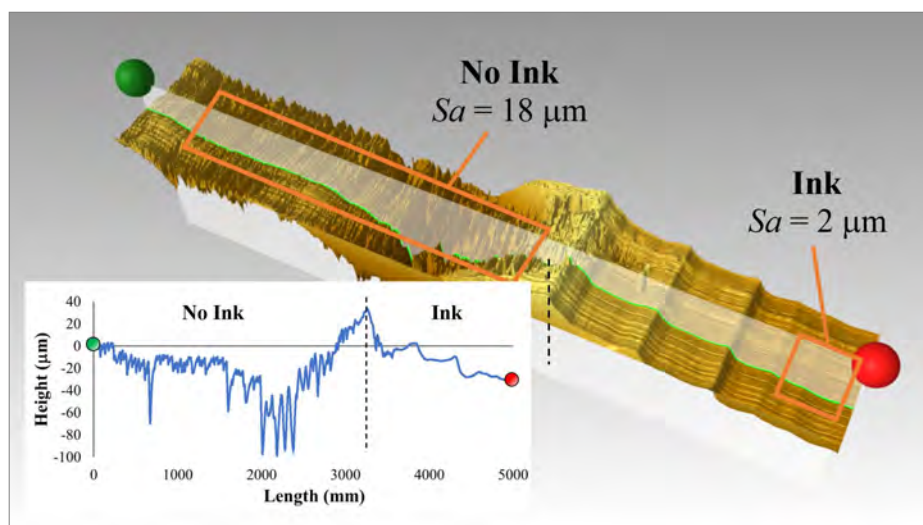


Fig. 12. Optical profilometer image of Ta surface produced by cutting with and without application of an ink-medium. The transition in the surface topography between the inked and non-inked regions is quite striking, indicating almost an order of magnitude improvement in surface topography due the MC effect. Sinuous flow (no ink) results in noticeable surface grooves with ridges and material pull-out. The latter can also be inferred from lack of tool marks on the cut surface. The  $S_a$  value in the no-ink region is  $\sim 18 \mu\text{m}$ . Application of ink results in a largely defect-free surface produced by active-cutting with tool marks. The  $S_a$  value in the inked region is  $\sim 2 \mu\text{m}$   $\alpha = 10^\circ$ ,  $h_0 = 40 \mu\text{m}$ ,  $V_0 = 2 \text{ mm/s}$ .



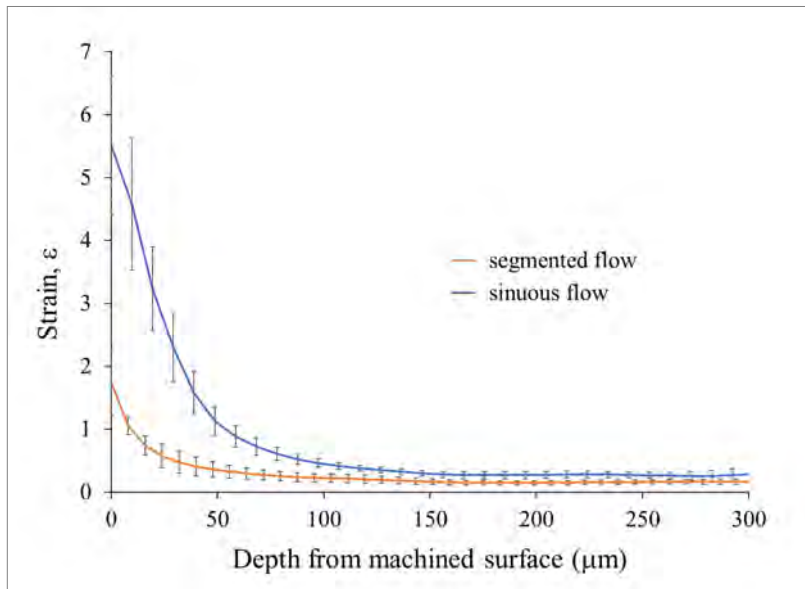


Fig. 13. Variation of residual plastic strain with depth from the machined Ta surface for the different flow modes. For sinuous flow (no ink), the average  $\varepsilon$  is  $\sim 5.5$  on the cut surface; while at a depth of  $\sim 90 \mu\text{m}$  from the cut surface,  $\varepsilon \sim 0.5$ . For segmented flow (ink medium), the average  $\varepsilon \sim 1.7$  on the cut surface, while  $\varepsilon \sim 0.5$  occurs at a depth of  $30 \mu\text{m}$  from the cut surface. Thus, both the strain at the surface and the depth of the deformed surface layer are both much smaller for the segmented flow case.  $\alpha = 10^\circ$ ,  $h_0 = 40 \mu\text{m}$ ,  $V_0 = 2 \text{ mm/s}$ .

### 3.5.3. Surface hardness

Nanoindentation using a Berkovich indenter was used to determine the hardness on the cut (machined) surface and subsurface. A  $13 \times 3$  array of indentations was made on the surface/subsurface created from the sinuous flow region, while an  $8 \times 3$  array was used in the segmented flow region. The indenter penetration used was  $2 \mu\text{m}$ , and the array spacing between rows and columns was  $12.5$  and  $100 \mu\text{m}$ , respectively. Fig. 14 shows a plot of the hardness vs. depth, obtained from the measurements. It is readily apparent that the surface produced by the sinuous flow has a much greater hardness than the one produced by the segmented flow (ink).

For example, in the sinuous flow case, the hardness is  $\sim 4.3 \text{ GPa}$  at a depth of  $10 \mu\text{m}$  from the surface; this may be considered as the machined surface hardness. This is consistent with the very large plastic strains ( $\varepsilon \sim 5.5$ ) measured on the cut surface in the sinuous flow case (Fig. 13). The hardness is seen to decrease gradually with depth from the machined surface, but even at a depth of  $\sim 200 \mu\text{m}$  it is greater than the bulk Ta hardness of  $\sim 2 \text{ GPa}$ . In contrast, for the segmented flow, the hardness on the cut surface is  $\sim 2.2 \text{ GPa}$  (Fig. 14), which is very close to the bulk Ta hardness; and the surface strain is  $\varepsilon \sim 1.7$ . Thus the MC effect causes very little strain hardening of the Ta workpiece surface during cutting, consistent with the reduced level of strain ( $\varepsilon \sim 1.7$ ) measured on this surface (Fig. 13). The results point to a means of producing “strain-free” or “minimally strained (damaged)” surfaces utilizing the MC effect.

### 3.5.4. Chip hardness

To analyze chip hardness, nanoindentation with a Berkovich indenter was used. The chip was cold mounted using Lecoset 100. This acrylic resin-based mount constrained the chip at its periphery, preventing buckling and slippage. The sample ‘puck’ was also supported by a stainless steel base. The indentation penetration depth was  $\sim 2 \mu\text{m}$ . By ensuring that the chip dimensions in each direction were at least 8 times greater than the corresponding indent dimensions, any substrate/mount effect on chip hardness was eliminated. A total of 18 indentations were made in the sinuous flow portion of the chip: 7 indentations including the origin ( $200 \mu\text{m}$  apart) were made vertically (y-axis in Fig. 15), 5 indentations ( $200 \mu\text{m}$  apart) were made horizontally (x-axis) to the right of the origin, and 6 indentations ( $140 \mu\text{m}$  apart) were made along a  $45^\circ$  diagonal. For the segmented flow case, hardness was sampled at three locations along the chip, towards each end and in the middle. A vertical line consisting of 3 indentations,  $50 \mu\text{m}$  apart, was made at each sampling site.

Fig. 15 is a nanohardness contour map for the chip that combines the data from the sinuous and segmented flow regions. The chip hardness values mirror the corresponding workpiece surface hardness. For the sinuous-flow chip, the highest hardness ( $\sim 4.5 \text{ GPa}$ ) is measured in the region immediately adjoining the tool rake face. This value is close to that measured on the corresponding workpiece surface. The hardness is seen to steadily decrease with distance from the rake face into the chip. The hardness pattern is consistent with the folding behavior revealed by the *in situ* imaging. As the chip is being formed, folds are continually added to the developing fan-like structure. The addition of each fold compresses the material in contact with the rake face, resulting in higher hardness. In the segmented flow portion of the chip, the hardness is smaller ( $\sim 3.2 \text{ GPa}$ ) and nearly uniform throughout.

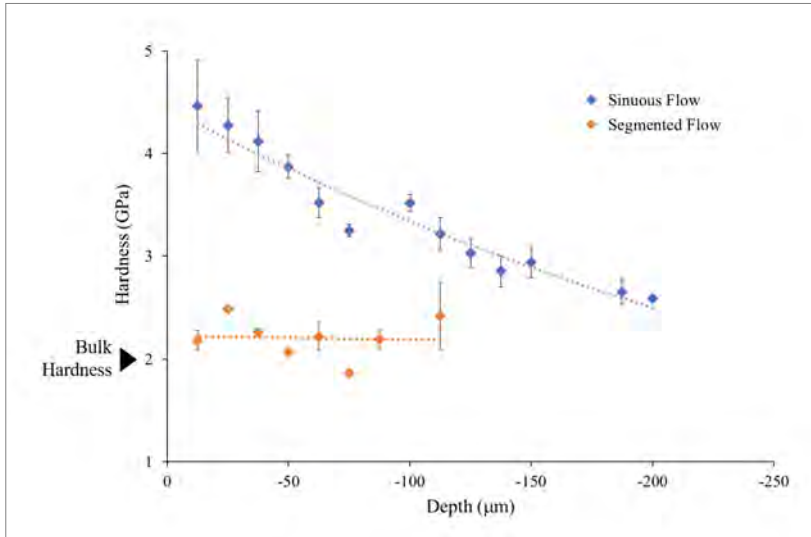


Fig. 14. Variation of nano-hardness with depth from the machined surface for Ta surfaces produced by the two flow modes. Near the cut surface, the hardness is  $\sim 4$  GPa for the surface produced by sinuous flow whereas it is only  $\sim 2$  GPa for the surface produced by segmented flow. The latter hardness is approximately the same as the initial bulk Ta hardness. This suggests negligible straining of the surface when cutting with the ink applied, pointing also to a means for producing “strain-free” surfaces.  $\alpha = 10^\circ$ ,  $h_0 = 40 \mu\text{m}$ ,  $V_0 = 2 \text{ mm/s}$ .

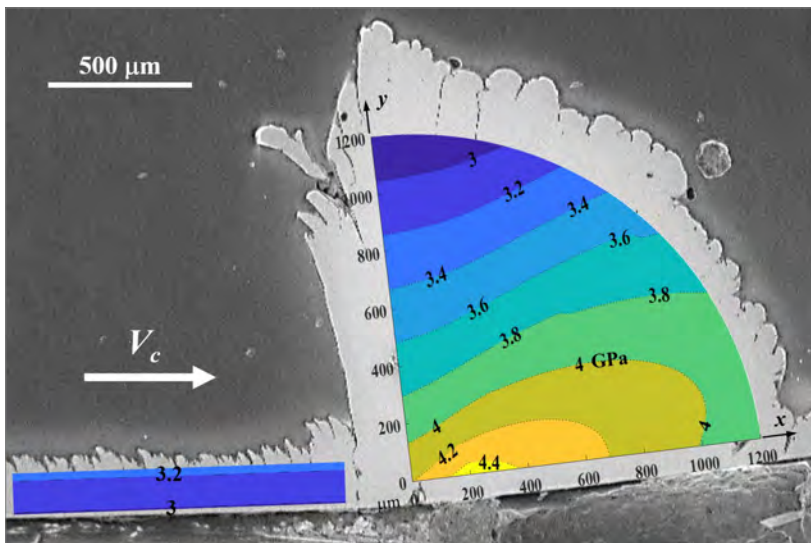


Fig. 15. Contour map of nano-hardness of Ta chip. The workpiece was partially uncoated and partially inked along its cutting length. For the sinuous flow portion of the chip (right, uncoated), the hardness is greatest in the region in contact with the tool rake face. For the segmented flow case (left, inked), the hardness is uniform throughout the chip ( $\sim 3$  GPa) and much less than in the sinuous flow case.  $\alpha = 10^\circ$ ,  $h_0 = 50 \mu\text{m}$ ,  $V_0 = 2 \text{ mm/s}$ .

#### 4. Discussion

Our *in situ* high-speed imaging of chip formation, complemented by force measurements, has revealed key aspects of material flow in cutting of Ta and the reason why Ta, although soft, is very difficult to cut. Chip formation in Ta, as in annealed Cu and Al, occurs by large-amplitude folding with the chip made up of a stack of folds (Figs. 3 and 4). This is revealed in the streakline pattern which shows a highly sinewy flow with significant vortex-like components (Fig. 5f) – this flow is very much similar to that of the sinuous flow mode first uncovered in cutting of Cu and Al [15,16]. The severity of the folding is however much greater in the Ta than in the Cu and Al, and there are also important differences in the folded chip morphology. In the case of Cu and Al, the deformed chip thickness is relatively constant, but the chip free surface has continuously recurring mushroom-like structures [16]. Each of these mushroom structures results from a fold and the folds themselves are stacked up one on top of the other to constitute the chip. However, in the Ta, the deformed chip progressively increases in thickness during cutting due to a piling-up of folds in the form of a fan-like structure (Fig. 5f); this results in a chip segment comprised of numerous folds, i.e., a folded chip segment. When such a folded segment becomes very thick (Figs. 3a and 4a), it fractures due to the forces reaching very large values; this deformation/fracture process then repeats resulting in the chip consisting of a series of thick folded segments separated by very local regions of fracture. This is to be contrasted with the vertical stacking of the recurring folds in Cu and Al. The fan-like structure of the folded chip in Ta also results in a different type of strain distribution within the chip compared to the Cu and Al. In Ta, the strain is concentrated near the tool tip which serves as the apex of the fan, whereas it is more distributed and less heterogeneous in the Cu and Al. The sinuous flow with folding is characterized by extensive redundant deformation and high strains (4–10), which explains the very large forces observed in cutting of Ta and the poor machinability of this material. Also, since Ta is a bcc system, the observation of sinuous flow in this system provides further evidence for its generality with the class of strain-hardening metals.



It should be noted that the occurrence of the sinuous flow mode in cutting, like other flow modes (e.g., laminar, shear banding, segmented), depends on certain parameters. Prior work with Cu and Al has shown that sinuous flow can be reduced and even suppressed by deforming the workpiece to moderate or large strains prior to the cutting, or by using tools of large positive rake angle. However, these solutions may not be feasible in practice. For example, in annealed Ta, laminar flow with a shear plane is observed only at rake angles of 30° and beyond (more positive). Unfortunately, this is not a suitable cutting condition, given the high tool wear and propensity for tool fracture at large positive rake angles. Based on the prior observations, a suggestion has been made that interpretation of the occurrence of specific flow modes in cutting of metals will require consideration of flow stability [18]. In this framework, the key parameters determining flow stability, and, by extension, the prevalent flow mode, are initial workpiece deformation state, strain rate and temperature. It will be interesting to examine Ta chip formation in this flow stability framework.

Although the sinuous flow is more severe in Ta, the folding nonetheless results in the same type of mushroom-shaped features on the chip free surface (Fig. 6) as observed in Cu and Al. The interfaces between successive mushroom features resemble notches. When cutting in the presence of surface-adsorbing (SA) media, these notches give way for cracks to propagate, thereby transitioning sinuous flow into segmentation flow. The disruption of sinuous flow by segmented flow strongly resembles a local ductile-to-brittle transition that is affected by the SA media, with attendant large drop (>75%) in the cutting forces (Fig. 10). These observations, together with the earlier work on Cu and Al [17,18, 28], strongly suggest that the local ductile-to-brittle transition mediates the MC effect vis-à-vis deformation, and that the segmentation flow mode is efficient from an energy standpoint.

In Ta, the folds are relatively continuous and run straight across the width of the chip (Fig. 3a and b) in contrast to the meandering folds observed in Al and Cu. Even in some instances where they are interrupted, or interlaced, with other folds, there are no breaks that occur along the length of individual folds. This continuity of the folds largely explains the periodicity of the segmentation when cutting in presence of the SA media, and the relative consistency in segment shape across the width of the chip.

While various details of the micromechanics of the flow transition and the MC effect are still being worked out, we can highlight some of the necessary conditions needed for this effect to be manifest, based on the current observations and others made earlier with Cu and Al. Firstly, sinuous flow with large redundant deformation should mediate the chip formation (absent the medium). Secondly, the notches between incipient folds play an important role in triggering the fracture and segmentation. Thirdly, and most important, are the changes in surface properties of the metal that are caused by the medium. We address this last point in greater detail below.

It is tempting to attribute the ductile-to-brittle transition to some form of metal corrosion that is caused by the SA medium. However, the observance of the MC effect in Ta dispels this assertion, as Ta is one of the most corrosion-resistant metals known. Since Ta is immune to attack by most acids, any corrosive action by the Sharpie marker ink is highly improbable. Instead, strong adsorption of SA media to the metal surface is likely the requisite condition. It is well-known that adsorbates can change the surface energy of the “metal surface”. This offers a route to explaining the observed brittle behavior by invoking a reduction in surface energy ahead of incipient crack tips, during the chip formation process, *a la* Griffith. While attractive again at first sight, this is extremely unlikely given that one will have to invoke implausible permeation mechanisms to explain ink penetration into the metal. That leaves the only other thermodynamic parameter in solids – surface stress – that is affected by adsorption as the probable cause. Organic molecules such as those present in the ink when adsorbed onto metal surface are known to cause changes in the surface stress [45]. This stress, analogous to a residual stress, can be of sufficient magnitude, when amplified by the crack-like features such as seen here, so as to cause fracture (segmentation). We hope to address the mechanics of this phenomenon in future papers.

Since adsorption is believed to be critical to the MC effect, additional considerations (e.g., thermal effects on adsorbate) must be made when choosing SA media for higher cutting speeds. However, we have identified media (e.g., protein rich media, cow’s milk) that suppress sinuous flow at higher cutting speeds for a range of ‘gummy’ metals and alloys. While this aspect is beyond the scope of this article, an in-depth treatment of the MC effect at high cutting speeds will be the topic of a future paper.

Our experiments point to many benefits that can be realized via use of the MC effect with highly strain-hardening metals. In no order of importance, they range from improved surface quality to improved cutting performance. With regards to quality, it has been demonstrated that the MC effect can significantly improve the poor surface finish that results from sinuous flow (absent the medium). Besides finish, other elements of machined surface quality are also positively impacted: major reduction in residual plastic strain (Fig. 14), suppression of tears and material pull-out, and minimal surface hardening. In fact, the machined surface hardness is practically the same as that of the bulk Ta, see Fig. 15. In terms of cutting performance, the substantial cutting (>75% reduction) and thrust force reductions realized, should be beneficial for tool life and process quality. Lastly, a larger range of cutting parameters become available for the cutting, such as using smaller positive rake angles. More broadly, the MC effect provides a simple route for effecting extraordinary broad improvements in cutting of gummy metals.

## 5. Conclusions

Using high-speed *in situ* imaging, we show that the extreme ‘gummy’ behavior of the refractory metal, tantalum, in cutting is due to sinuous flow, with large-amplitude folding, driving chip formation. The chip produced by sinuous flow is composed of a series of folds that are stacked together, a morphology that is quite distinct from that of a conventional chip produced by laminar flow with well-defined shear zone/plane. Furthermore, the folding in Ta is much more severe, and has a different morphology, than that observed in other gummy metals like commercially pure Al and Cu. Various key attributes of the sinuous flow such as large heterogeneous strains (4–10), extensive redundant deformation and large energy dissipation, have been quantified via the high-speed imaging and force measurements. The occurrence of the sinuous flow in a bcc system further attests to the generality of this deformation mode and to the close connection between this flow mode and the machinability attribute of “gumminess”.

When the cutting is done in the presence of a surface-adsorbing (SA) medium, e.g., permanent marker ink, the sinuous flow is disrupted and replaced by a segmented flow mode, via a local ductile-to-brittle transition in the flow in the deformation zone – a mechanochemical (MC) effect. The segmented flow gives rise to a saw-tooth chip. The MC effect causes a fundamental change in flow dynamics and chip morphology. Importantly, there is a large (>70%) drop in the cutting force and specific energy, another key defining attribute of the MC effect. The MC effect produces major improvements in the quality of the cut surface – smoother surface topography, reduced material pull-out, and minimal plastic straining on the surface. Thus, use of an appropriate SA medium and the MC effect offers a promising route for increasing the machinability of Ta by disrupting the sinuous flow. This approach is likely to be of value even for cutting other gummy metals like Nb and ferritic stainless steels (bcc), and Ni alloys and austenitic stainless steels (fcc).

The severity of the folding and extreme sinuous flow in Ta offer opportunities to better understand the coupling between flow dynamics and the MC effect, even more so than is feasible with other metals like Al or Cu. Wide-ranging application of mechanochemically-assisted machining in industrial practice will benefit from fundamental understanding of adsorbate-metal interactions, for this will help in selection of the right type of adsorbate molecules and in the means of their application. Ongoing work also seeks, among other things, to demarcate the parameter space (e.g., speed) wherein the MC effect is prevalent, and further elucidation of the flow micromechanics, especially the coupling between surface plasticity and thermodynamics of adsorbed films.

## Acknowledgements

JMD would like to acknowledge support from the DoD, Naval Surface Warfare Center, Crane Division, under the NISE Program and the DoD SMART Scholarship-for-Service Program. The work at Purdue University was supported in part also by NSF grants CMMI 1562470 and DMR 1610094.

Supplementary data to this article can be found online at <https://doi.org/10.1016/j.ijmachtools.2020.103607>

## APPENDIX A. Properties of permanent marker ink and ink application to the surface

It is worthwhile to briefly discuss some of the properties of Sharpie permanent marker ink and its interaction with surfaces. Permanent marker offers several attractive properties as an SA medium. First, the marker is considered relatively benign to the health of the user. In fact, the markers are now exempt from the requirement of a Safety Data Sheet (SDS) per the updated U. S. Occupational Safety and Health Administration (OSHA) Globally Harmonized System of Classification and Labeling of Chemicals (GHS) Hazard Communication Standard which took effect in June 2015 [46]. They also bear The Art and Creative Materials Institute, Inc. (ACMI) Approved Product (AP) Non-Toxic Seal, having been “certified in a toxicological evaluation by a medical expert as containing no materials in sufficient quantity to be toxic or injurious to humans, including children, or to cause acute or chronic health problems” [47,48]. Prior published Material Safety Data Sheets (MSDS) state the markers consist of butanol (71-36-3), propanol (71-23-8), diacetone alcohol (123-42-2), ethanol (64-17-5), pigments, dyes, and additives [47].

In addition to being benign, the low viscosity of the ink gives rise to two other desirable qualities – gap filling and planarization – both representative of the wetting ability of the ink [49]. Gap filling can be attributed to capillary action [50], while planarization results from the behavior of the ink under a gravitational field. Gap filling and planarization help ensure adequate coating of the surface of the workpiece, whose roughness is largely based on the surface preparation operation used. Coating of low and moderate-aspect ratio structures on the workpiece surface with few pores is virtually certain [49].

To gain a greater understanding of the coating thickness that a Sharpie permanent marker provides, a plate of glass was marked (coated) regularly with lines of ink for a total of four lines (Figure A.1). The number of writing strokes was increased with each line, resulting in lines with 1-stroke, 2-strokes, 3-strokes, and 4-strokes of ink. Figure A.1 is a profilometry-generated image of the ink lines, along with a profile from a 2D slice across the width of the lines. Average thickness for the ink coatings was approximately 0.1, 0.2, 0.4, and 0.7  $\mu\text{m}$  for the 1-stroke, 2-stroke, 3-stroke, and 4-stroke lines, respectively. Recalling that the spatial resolution of the high-speed imaging system is 1.4  $\mu\text{m}$  per pixel, the ink layer is indiscernible during imaging.

It should be noted that the surface roughness on the workpiece ( $S_a \sim 2 \mu\text{m}$ ) was considerably greater than that of the applied ink layer ( $\sim 200 \text{ nm}$ ). As an example, Figure A.2 is a profilometry-generated image of a Ta surface with arithmetical mean height  $S_a$  of 0.93  $\mu\text{m}$  and root mean square height  $S_q$  of 1.17  $\mu\text{m}$ ; this surface had four lines of ink applied, each with varying number of strokes. The first line (1-stroke) is not visible at all. The locations of the other three lines are discernible, but not entirely visible. Even for this workpiece surface roughness, approximately half the  $S_a$  in the experiments, much of the ink is concealed. Based on these considerations, 2-stroke lines ( $\sim 200 \text{ nm}$  thick ink films) were used in the experiments to ensure adequate coverage.



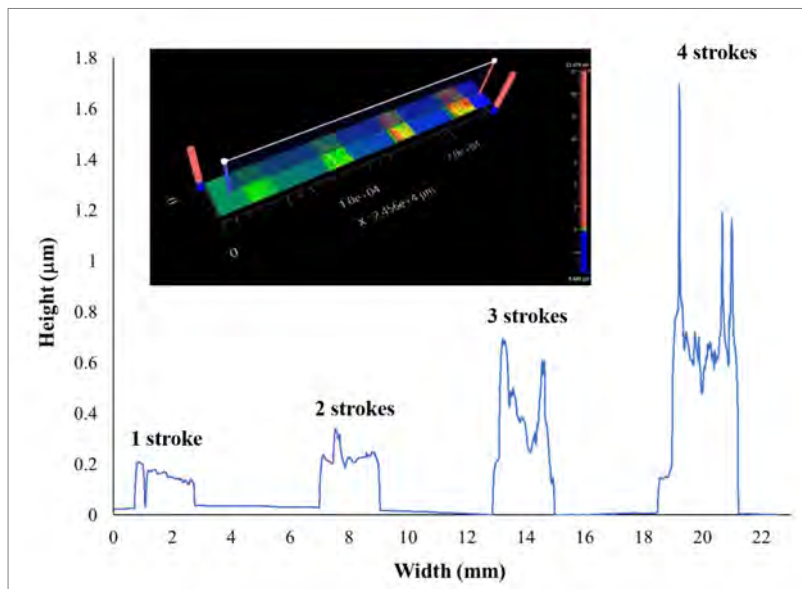
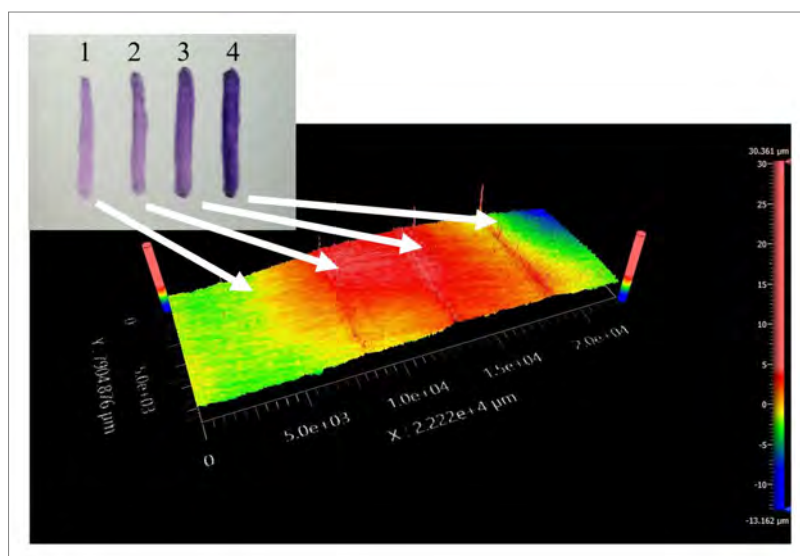


Fig. A.1. Optical profilometer image of glass microslide surface coated using a Sharpie permanent marker. From left-to-right, the first ink line was created with one writing stroke; thereafter, the number of writing strokes was incrementally increased by one. This imaging was used to measure the ink film thickness. In the cutting experiments, two strokes of the marker pen were used to ink the Ta surface, resulting in a film thickness of ~200 nm.

Fig. A.2. 3D optical profilometer image of Ta workpiece surface (arithmetic mean height  $S_a$  of 0.93  $\mu\text{m}$ ) to which four lines of Sharpie permanent marker ink have been applied. Number of writing strokes (single stroke, extreme left) is increased incrementally stepwise from left-to-right. The ink film adheres tightly to the surface topography and hence its presence is largely obscured by the background surface roughness.



## References

- 1) A.G. Ekeberg, Of the properties of the earth yttria, compared with those of glucine; of fossils, in which the first of these earths is contained; and of the discovery of a new substance of a metallic nature (tantalum), J. Nat. Philos. Chem. Arts. 3 (1802) 251–255.
- 2) S. Venetsky, Tales about Metals, Mir Publishers, 1988.
- 3) Homer, the Odyssey, Open Road Media, ProQuest Ebook Central, 2017. <http://ebookcentral.proquest.com/lib/purdue/detail.action?docID 4828841>.
- 4) Z.Y. Wang, K.P. Rajurkar, J. Fan, G. Petrescu, Cryogenic machining of tantalum, J. Manuf. Process. 4 (2002) 122–127.
- 5) P.A. Schweitzer, Corrosion and Corrosion Protection Handbook, Marcel Dekker, New York, NY, 1989.
- 6) K. Sakai, K. Shintani, H. Kato, Study on the cutting mechanism of tantalum materials, Proc. JSPE Spring Conf. (2011) 239–240 (in Japanese).
- 7) K. Shintani, K. Sakai, H. Kato, Study on cutting work of tantalum materials, Proc. JSPE Autumn Conf. (2011) 201–202 (in Japanese).
- 8) K. Shintani, K. Wakabayashi, Y. Higuchi, H. Sumiya, Study on cutting of tantalum materials with nano-polycrystalline diamond tool, Proc. JSPE Autumn Conf. (2012) 199–200 (in Japanese).
- 9) S.D. Cramer, B.S. Covino, Corrosion of tantalum and tantalum alloys, ASM Handb. Corros. Mater. 13B (2005) 337–353.
- 10) K.J. Schulz, N.M. Piatak, J.F. Papp, Niobium and Tantalum, 2017. Reston, VA, <http://pubs.er.usgs.gov/publication/pp1802M>.
- 11) W.S. de Rosset, Explosively Bonded Gun Tube Liner Development (ARL-CR-0771), U. S. Army Research Laboratory, Aberdeen Proving Ground, MD, 2015.
- 12) Defense metals information center, Machining of Superalloys and Refractory Metals (DMIC Memorandum 134), Battelle Memorial Institute, Columbus, OH, 1961.
- 13) L.J. Lazarus, Topical report: tantalum – 2.5% tungsten machinability testing (KCP- 613-8615), Honeywell Fed, Manuf. Technol. (2009) 12–13.
- 14) W.R. Barton, Columbium and Tantalum: A Materials Survey (Information Circular 8120), U. S. Dept. of Interior, Bureau of Mines, Washington, DC, 1962.
- 15) A. Udupa, K. Viswanathan, Y. Ho, S. Chandrasekar, The cutting of metals via plastic buckling, Proc. R. Soc. A Math. Phys. Eng. Sci. 473 (2017) 20160863.
- 16) H. Yeung, K. Viswanathan, W.D. Compton, S. Chandrasekar, Sinuous flow in metals, Proc. Natl. Acad. Sci. U.S.A. 112 (2015) 9828–9832.
- 17) A. Udupa, K. Viswanathan, M. Saei, J.B. Mann, S. Chandrasekar, Material- independent mechanochemical effect in the deformation of highly-strain- hardening metals, Phys. Rev. Appl. 10 (2018) 1.

- 18) A. Udupa, T. Sugihara, K. Viswanathan, S. Chandrasekar, Altering the stability of surface plastic flow via mechanochemical effects, *Phys. Rev. Appl.* 11 (2019) 1.
- 19) R.J. Adrian, *Particle Image Velocimetry*, Cambridge University Press, Cambridge, 2011.
- 20) T. Kaneeda, M. Yamada, L. Anthony, Chip formation mechanism of pure Niobium plates in a superconducting accelerator cavities, *Proc. 13th Int. Conf. Eur. Soc. Precis. Eng. Nanotechnol. EUSPEN 2013* 2 (2013) 129–132.
- 21) F.M. White, *Fluid Mechanics*, fourth ed., WCB/McGraw-Hill, Boston, Mass., 1999.
- 22) H. Yeung, K. Viswanathan, A. Udupa, A. Mahato, S. Chandrasekar, Sinuous flow in cutting of metals, *Phys. Rev. Appl.* 8 (2017) 1–15.
- 23) R.F. Recht, Catastrophic thermoplastic shear, *J. Appl. Mech.* 31 (1964) 189–193.
- 24) D. Sagapuram, K. Viswanathan, A. Mahato, N.K. Sundaram, R. M'Saoubi, K. P. Trumble, S. Chandrasekar, Geometric flow control of shear bands by suppression of viscous sliding, *Proc. R. Soc. A Math. Phys. Eng. Sci.* 472 (2016).
- 25) R. Bejjani, M. Balazinski, H. Attia, P. Plamondon, G. L'E'sp'rance, Chip formation and microstructure evolution in the adiabatic shear band when machining titanium metal matrix composites, *Int. J. Mach. Tool Manufact.* 109 (2016) 137–146.
- 26) N.H. Cook, I. Finnie, M.C. Shaw, Discontinuous chip formation, *ASME Trans.* 76 (1954) 153–162.
- 27) M.S. Dargusch, S. Sun, J.W. Kim, T. Li, P. Trimby, J. Cairney, Effect of tool wear evolution on chip formation during dry machining of Ti-6Al-4V alloy, *Int. J. Mach. Tool Manufact.* 126 (2018) 13–17.
- 28) M. Saei, A. Udupa, K. Viswanathan, T. Sugihara, R. M'Saoubi, S. Chandrasekar, Controlling segmentation in cutting of metals, *CIRP Ann* 68 (2019) 41–44.
- 29) Mitsubishi Materials Corp, Technical information. [http://www.mitsubishicarbide.net/contents/mhg/enuk/html/product/technical\\_information/information/form ula4.html](http://www.mitsubishicarbide.net/contents/mhg/enuk/html/product/technical_information/information/form ula4.html), 2020. (Accessed 31 March 2020).
- 30) Metal cutting technology technical guide, Sandvik Coromant (2010).
- 31) A. Hijazi, V. Madhavan, A novel ultra-high speed camera for digital image processing applications, *Meas. Sci. Technol.* 19 (2008).
- 32) E.P. Gnanamanickam, S. Lee, J.P. Sullivan, S. Chandrasekar, Direct measurement of large-strain deformation fields by particle tracking, *Meas. Sci. Technol.* 20 (2009).
- 33) M.C. Shaw, *Metal Cutting Principles*, second ed., Oxford University Press, New York, 2005.
- 34) M.E. Merchant, Mechanics of the metal cutting process. I. Orthogonal cutting and a type 2 chip, *J. Appl. Phys.* 16 (1945) 267–275.
- 35) R. Roscoe, The plastic deformation of cadmium single-crystals, London, Edinburgh Dublin Philos. Mag. J. Sci. 21 (1936) 399.
- 36) A.F. Joffe, *The Physics of Crystals*, McGraw-Hill Book Co., Inc., New York, 1928.
- 37) P.A. Rehbinder, E.D. Shchukin, Surface phenomena in solids during deformation and fracture processes, *Prog. Surf. Sci.* 3 (1972).
- 38) D.H. Bangham, The Gibbs adsorption equation and adsorption on solids, *Trans. Faraday Soc.* 33 (1937) 805–811.
- 39) R.M. Latanision, A.R.C. Westwood, Surface- and environment- sensitive mechanical behavior, *Adv. Corros. Sci. Technol.* (1970) 51–145.
- 40) A.R.C. Westwood, R.K. Viswanadham, J.A.S. Green, Environment-sensitive mechanical behavior of oxides and oxide-coated metals, *Thin Solid Films* 39 (1976) 69–78.
- 41) F. Pusavec, A. Deshpande, S. Yang, R. M'Saoubi, J. Kopac, O.W. Dillon, I. S. Jawahir, Sustainable machining of high temperature Nickel alloy - inconel 718: Part 2 - chip breakability and optimization, *J. Clean. Prod.* 87 (2015) 941–952.
- 42) A. Chaudhari, Z.Y. Soh, H. Wang, A.S. Kumar, Rehbinder effect in ultraprecision machining of ductile materials, *Int. J. Mach. Tool Manufact.* 133 (2018) 47–60.
- 43) G.E. Dieter, *Mechanical Metallurgy*, Chapter 12, third ed., McGraw-Hill India, 2013.
- 44) T.H. Courtney, *Mechanical Behavior of Materials*, Chapter 12, second ed., Waveland Press, 2005.
- 45) G. Wu, H. Ji, K. Hansen, T. Thundat, R. Datar, R. Cote, M.F. Hagan, A. K. Chakraborty, A. Majumdar, Origin of nanomechanical cantilever motion generated from biomolecular interactions, *Proc. Natl. Acad. Sci. U.S.A.* 98 (2001) 1560–1564.
- 46) Newell Rubbermaid, Hazard Communication Compliance Declaration,
- 47) Newell Rubbermaid, Material Safety Data Sheet (MSDS #3000), 2012.
- 48) ACMI: the Art and Creative Materials Institute, What do the ACMI seals mean?, 2019. <https://acmiart.org/index.php/art-material-safety/safety-tips-what-you-need-to-know#3>. (Accessed 31 March 2020).
- 49) Y.C. Park, B.C. Park, S. Romankov, K.J. Park, J.H. Yoo, Y.B. Lee, J.M. Yang, Use of permanent marker to deposit a protection layer against FIB damage in TEM specimen preparation, *J. Microsc.* 255 (2014) 180–187.
- 50) J. Kim, M.W. Moon, K.R. Lee, L. Mahadevan, H.Y. Kim, Hydrodynamics of writing s. *Rev. Lett.* 107 (2011) 2–5.



**The 2021 Anders Gustaf Ekeberg Tantalum Prize  
will be awarded at the 62nd General Assembly to be  
held in London, UK, from November 14th to 17th.**





**RC INSPECTION**  
GROUP



**RC INSPECTION**  
INSPECTION SAMPLING

The RC Inspection Group offices are based around the globe and are active in each important, active economic centre and beyond. The Group offers management and team members with more than 30 years' experience and knowhow and therefore its clients benefit from services of the highest quality to be found in the fields of inspection, sampling, weight determination, maritime- and analytical services.

RC Inspection offers worldwide a complete spectrum of services on ores, minerals, concentrates, noble alloys, high purity-, base-, precious and rare earth metals, non-ferrous scrap, ferrous scrap, solid (bio)fuels, agricultural products and fertilizers, through a unique network of professionals.

The services are all performed according to ISO/IEC 17020 accreditation (RvA no.: I308) which ensures the clients of accurate and high quality results.

**Creating value through combining knowledge and experience.**



**RCI ANALYTICAL SERVICES**  
ANALYSIS

RC Inspection keeps the analysis in-house conducted by its group company RCI Analytical Services. The laboratories are to-date strategically located in The Netherlands, Ukraine and Mongolia.

They are equipped with the most modern and advanced instruments to drive accelerated turnaround times and up-to-the-minute reporting through a service driven approach and innovative use of technology.

The analysis are performed using all relevant modern analytical techniques and under full ISO/IEC 17025 accreditation :

RCI Analytical Services The Netherlands – RvA registration nr.: L611 and LME listed

RCI Asia Assayers Mongolia – MASM registration nr.: TL110

RCI Analytical Services Ukraine – GAS registration nr.: L.804.027

**METALS / MINERALS / ORES / CONCENTRATES / FERROUS SCRAP / NON FERROUS SCRAP  
SOLID FUELS / SOLID BIOMASS / FERTILIZERS / AGRICULTURAL / MARITIME SERVICE**

[WWW.RC-INSPECTION.COM](http://WWW.RC-INSPECTION.COM)

[OPERATIONS@RC-INSPECTION.COM](mailto:OPERATIONS@RC-INSPECTION.COM)

+31 (0)10 425 02 40





# Tantalum and niobium intellectual property update

*This information is taken from the European Patent Office ([www.epo.org](http://www.epo.org)) and similar institutions. Patents listed here were chosen because of their apparent relevance to tantalum and/or niobium. Some may be more relevant than others. Note that European patent applications that are published with a search report are 'A1', while those without a search report are 'A2'. When a patent is granted, it is published as a B document. Disclaimer: This document is for general information only and no liability whatsoever is accepted. The T.I.C. makes no claim as to the accuracy or completeness of the information herein.*

Title	Applicant(s)	Publication date
Publication #		

## TANTALUM

Semiconductor device, manufacturing method of semiconductor device and testing device		
<a href="#">US2021320184 (A1)</a>	ADVANTEST CORP [JP]	2021-10-14
Electro-optical device		
<a href="#">WO2021201130 (A1)</a>	TDK CORP [JP]	2021-10-07
Electrolytic capacitor having a tantalum anode		
<a href="#">US2021313118 (A1)</a>	GREATBATCH LTD [US]	2021-10-07
Nickel based superalloy braze filler		
<a href="#">US2021308809 (A1)</a>	SIEMENS ENERGY INC [US]	2021-10-07
Tantalum based alloy that is resistant to aqueous corrosion		
<a href="#">US2021301374 (A1)</a>	AIMONE PAUL R [US]; HINSHAW EVAN [US]	2021-09-30
Recovery method of tantalum		
<a href="#">KR20210107346 (A)</a>	ECO RECYCLING CO LTD [KR]	2021-09-01
Method for producing potassium tantalate particles, method for producing film, potassium tantalate particles, film, antireflective film, optical element, and optical apparatus		
<a href="#">WO2021187412 (A1)</a>	NIKON CORP [JP]; UNIV TOHOKU [JP]	2021-09-23
Nickel-based superalloy for manufacturing a part by powder forming		
<a href="#">US2021292873 (A1)</a>	SAFRAN [FR]	2021-09-23
Etching solution for selectively removing tantalum nitride over titanium nitride during manufacture of a semiconductor device		
<a href="#">SG10202107132Q (A)</a>	VERSUM MATERIALS US LLC [US]	2021-08-30
A method related to the performance improvement of Schottky diodes with an enhancement layer of silicon-carbon and thickness adjustable layer of tantalum nitride		
<a href="#">AU2021104234 (A4)</a>	HE JIACHEN [CN]; HOU XINYU [CN]; YI ZHIHAO [CN]	2021-09-09
Tantalum pentoxide based low-loss metasurface optics for UV applications		
<a href="#">US2021262077 (A1)</a>	UNIV MARYLAND [US]; GOVERNMENT OF US SECRETARY OF COMMERCE [US]	2021-08-26
Method for alloying aluminium with tantalum		
<a href="#">RU2753630 (C1)</a>	FEDERALNOE GOSUDARSTVENNOE BYUDZHETNOE UCHREZHDENIE NAUKI ... [RU]	2021-08-18

## NIOBIUM

Ultra high strength and high ductility steel sheet having excellent yield ratio and manufacturing method for same		
<a href="#">US2021317554 (A1)</a>	POSCO [KR]	2021-10-14
Electrophotographic photosensitive member, process cartridge and electrophotographic apparatus		
<a href="#">US2021318628 (A1)</a>	CANON KK [JP]	2021-10-14
Balance spring for a clockwork and the method for its manufacture		
<a href="#">RU2756785 (C1)</a>	NIVAROX SA [CH]	2021-10-05
Cold-rolled and heat-treated sheet steel and method for manufacture thereof		
<a href="#">RU2757020 (C1)</a>	ARCELORMITTAL [LU]	2021-10-08
Method for producing nanocomposites of niobium and tantalum carbides in the carbon matrix - NbC/C and TaC/C		
<a href="#">RU2756759 (C1)</a>	ILIN EVGENII GRIGOREVICH [RU]	2021-10-05
Secondary battery, battery pack, and vehicle		
<a href="#">US2021296631 (A1)</a>	TOSHIBA KK [JP]	2021-09-23
Electroplating of niobium titanium		
<a href="#">US2021296749 (A1)</a>	IBM [US]	2021-09-23

Negative electrode, secondary battery, battery pack, and vehicle US2021288306 (A1) TOSHIBA KK [JP]	2021-09-16
Cesium-niobium-chalcogenide compounds and semiconductor devices including the same US2021269326 (A1) TRINITY COLLEGE DUBLIN [IE]; QATAR FOUND EDUCATION SCIENCE ... [QA]	2021-09-02
Piezoceramic material RU2753917 (C1) AKTSIONERNOE OBSHCHESTVO NAUCHNO ISSLEDOVATELSKIY INST... [RU]	2021-08-24
High-strength structural steel WO2021167496 (A1) JOINT STOCK COMPANY UNITED ENGINE CORP JSC UEC [RU]	2021-08-26
Method for manufacturing rods from superelastic alloys based on the Ti-Zr-Nb system RU2753210 (C1) OBSHCHESTVO S OGRANICHENNOJ OTVETSTVENNOSTYU SPF BIOLAB [RU]	2021-08-12

## Diary of industry events\*

- IAEA's 43rd TRANSSC meeting, November 1st - 5th 2021
- **T.I.C.'s 62nd General Assembly and 2021 AGM, London, UK, November 14th - 17th 2021**
- FORMNEXT, Frankfurt, Germany, November 16th - 19th 2021
- International Workshop on Critical Materials, online, November 16th - 18th 2021
- Tarantula (Month 30), December 17th 2021
- Investing in African Mining Indaba, Cape Town, South Africa, May 9th - 12th 2022
- IAEA's 44th TRANSSC meeting, (tbc) June 2022
- Tarantula (Month 36), (tbc) June 2022
- **T.I.C.'s 63rd General Assembly and 2022 AGM, Geneva, Switzerland, October 16th - 19th 2022**

\* correct at time of print

## Member company updates

### Changes in member contact details

Since the last edition of this newsletter the following changes have been made to delegate contact details:

- **Australian Strategic Materials Ltd** has a new delegate, Ms Linda Cardillo. She can be contacted on [lcardillo@asm-au.com](mailto:lcardillo@asm-au.com).
- **Jiujiang Jinxin Non-ferrous Metals Co. Ltd** has a new address: No.018, QinHu Avenue, BinJiang East Road, XunYang District, JiuJiang City, JiangXi Province (JiuJiang Petrochemical Industrial Park), China. All other details remain unchanged.
- **Pilbara Minerals Limited**. The delegate has a new email address: [agray@pilbaraminerals.com.au](mailto:agray@pilbaraminerals.com.au).
- **Roskill Information Services Ltd** has a new delegate, Ms Jessica Roberts. She can be contacted on [Jessica@roskill.com](mailto:Jessica@roskill.com).

### Changes in T.I.C. contact details

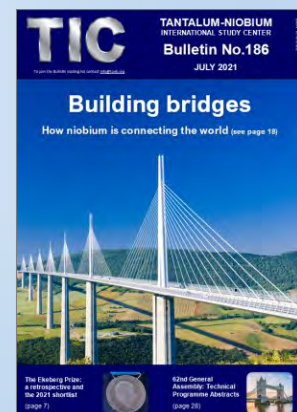
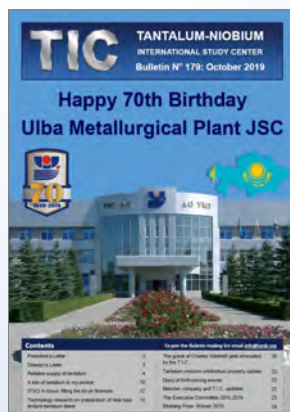
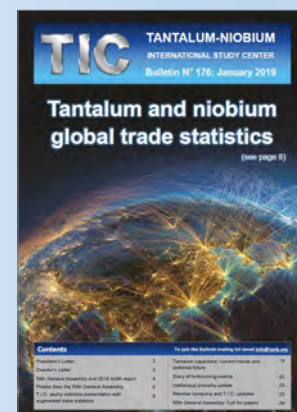
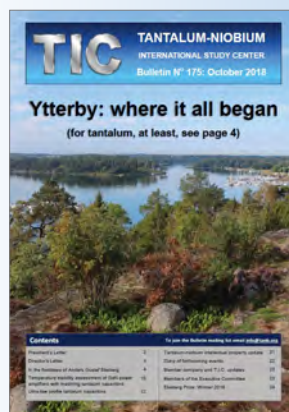
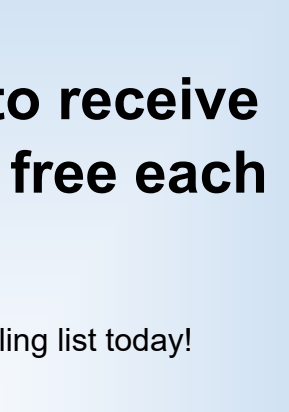
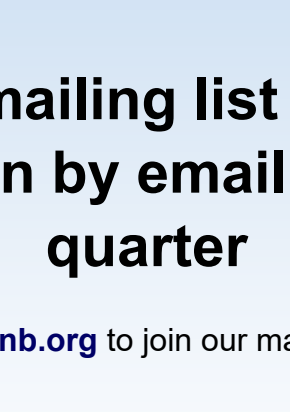
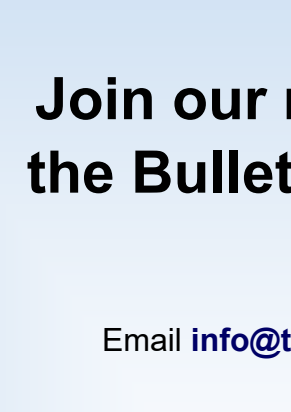
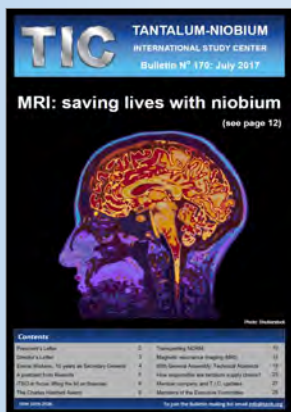
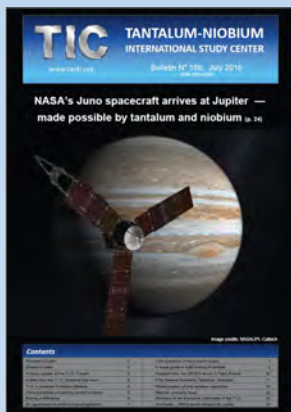
- Ian Margerison is the new Executive Marketing Manager. He can be contacted on [ian.margerison@tanb.org](mailto:ian.margerison@tanb.org).

The Bulletin is published by the Tantalum-Niobium International Study Center (T.I.C.); ISSN 1019-2026. Editor: Roland Chavasse; Production Director: Emma Wickens. The T.I.C. can be contacted at [info@tanb.org](mailto:info@tanb.org); [www.tanb.org](http://www.tanb.org); +32 2 649 51 58, or at the registered address: Chaussée de Louvain 490, 1380 Lasne, Belgium.

The T.I.C. is an international, non-profit association founded in 1974 under Belgian law that represents around 90 members from over 30 countries involved with all aspects of the tantalum and niobium industry. The T.I.C. is managed by an Executive Committee elected from the membership and representing all segments of the industry. Corporate membership costs EUR 2750 per year and full details of benefits are available at [www.TaNb.org](http://www.TaNb.org)

**Disclaimer:** Tantalum-Niobium International Study Center (T.I.C.) has made every effort to ensure that the information presented is technically correct. However, T.I.C. does not represent or warrant the accuracy of the information contained in the Bulletin or its suitability for any general or specific use. The reader is advised that the material contained herein is for information purposes only; it should not be used or relied upon for any specific or general application without first obtaining competent advice. The T.I.C., its members, staff and consultants specifically disclaim any and all liability or responsibility of any kind for loss, damage, or injury resulting from the use of the information contained in this publication.





Join our mailing list to receive the Bulletin by email, free each quarter

Email [info@tanb.org](mailto:info@tanb.org) to join our mailing list today!



# Editor's farewell

London, UK

Dear T.I.C. Members and stakeholders,

I hope that you, your family and friends are staying well during these challenging times. As I write this, here in London the annual "London Metals Week" is taking place and for the first time in over 18 months face-to-face meetings appear to be the norm again, and what a relief that is, too!

The return towards normality is great news for the Association's 62nd General Assembly (conference and annual general meeting) which will take place here next month. The Meetings Subteam, led by Dr Daniel Persico and with support from Emma Wickens and myself, has assembled a truly world-class group of speakers and panellists and it should be an event to remember for all the right reasons. Full details of the event can be found on our website at <https://www.tanb.org/event-view/62nd-general-assembly>, including the general information, plenary schedule and booking form. Non-members are welcome to attend this event.



London, UK, home to the T.I.C.'s 62nd General Assembly

## Moving on

Effective November 13th, I will be leaving the T.I.C. after six enjoyable years which, with the support of the Executive Committee and members, has been a time of considerable investment and progress at the Association. Our outreach has never been wider or our internal structures stronger than they are today; our membership levels have been stable throughout and we have taken the General Assembly to central Africa for the first time, a long-held dream for many members. Together, we have achieved a great deal.

It gives me great pleasure to welcome my replacement, Ian Margerison, to the T.I.C. team. Ian has spent many years as part of the T.I.C. community as the delegate for Metalysis, and he knows the Association well. He helped organise the 54th General Assembly and was a member of the Executive Committee and was even chair of the Marketing Subteam for a while, too. I can't think of anyone better to take over as Executive Marketing Manager and Editor of the Bulletin.

It has been my pleasure to work with the membership and Executive Committee as both Director and Executive Marketing Manager on initiatives that were important to the industry and to the membership as a whole. The work was always interesting and I've made many new friends along the way. I have also learned a great deal about two fascinating elements and it is my sincere hope that I have been able to share some of that knowledge with the readers of the Bulletin.

I extend my best wishes for the future to the membership, Emma, Ian and Executive Committee moving forward.

I look forward to our paths crossing again in due course, but, until then, look after yourself and those dear to you.

Kind regards,

Roland



T.I.C.'s incoming and outgoing Bulletin Editors, respectively Ian Margerison (left) and Roland Chavasse, pictured in September 2019 at Metalysis.



EST. 1990

**EXOTECH**  
WORLD CLASS METALLURGY

ISO 9001:2015

ACCOMPLISHING THE DIFFICULT.  
**MAKING A DIFFERENCE.**

**STOCKING SUPPLIER OF RECYCLED**  
Pure and Alloy

Tantalum  
Niobium  
Zirconium  
Hafnium

Molybdenum  
Tungsten  
Vanadium  
Other Exotics

**PRODUCER OF**  
High Purity Chromium Powder  
Synthetic Tantalum Concentrates

**SPECIALIZING IN**  
High Purity Sputter Target Alloys  
Recycling Unique Tantalum Refinery

+1 (954) 917-1919

[WWW.EXOTECH.COM](http://WWW.EXOTECH.COM)

[EXOTECH@EXOTECH.COM](mailto:EXOTECH@EXOTECH.COM)